SCAP-1D : A Spatial Correlation Assessment Procedure from unidimensional discrete data

Romain Clerc, Mestapha Oumouni, Franck Schoefs

SCAP-1D : A Spatial Correlation Assessment Procedure from Unidimensional Discrete Data

Romain Clerc*, Mestapha Oumouni, Franck Schoefs

Institute for Research in Civil and Mechanical Engineering (GeM), UMR CNRS 6183
Université de Nantes, chemin de la Houssinière, 44322 Nantes cedex 1

* corresponding author : romain.clerc@univ-nantes.fr

Abstract: *Optimal placement of Non-destructive Testing sensors is essential for structure diagnosis as it allows to get maximum information about degradation at minimum cost. Latest optimization methods consider spatial variability of quantities of interest and thus strongly rely on correlation lengths assessment. However, this estimation is usually done with straightforward techniques on raw data, which may not satisfy the required hypotheses of stationarity and ergodicity and induce important mis-estimations.*

In this paper, we propose a Spatial Correlation Assessment Procedure (SCAP-1D) which allows to rigorously assess correlation length of a quantity of interest modeled as a piecewise-trend-stationary Gaussian-Random-Field (GRF). The procedure is applicable to unidimensional limited data and comprises two steps. First, the correlation length is assessed through an iterative algorithm including mean changepoints detection. Then, stationarity, ergodicity and normality are tested to validate both the model and estimations.

In numerical studies, we demonstrate the ability of our procedure to accurately estimate correlation length of a GRF in the cases of constant, stepped and bilinear mean, with performance ranges assessment. Applications to experimental Half-Cell Potential measurements with effective mean and slope steps validate the capacity of our method to precisely determine mean changepoints and correlation length on real data.

Keywords: *Stochastic Fields; Spatial Variability; Piecewise-trend-stationarity; Mean Changepoints Detection Identification; Non-Destructive Techniques; Maximum Likelihood Estimation*

1 INTRODUCTION

Since the end of the 20th and the beginning of the 21st century, concrete structures maintenance has become a major economic and security issue [1]. Initially designed with weak aging models and poor control processes for 50 to 70-year service lives, they require numerous inspections and even reparations to limit their degradation and ensure their serviceability state.

Employed for decades, the usual maintenance strategy follows three steps. Visual inspection is performed by an expert engineer who defines the critical zones of the structure. Core samples or Non-Destructive Testing (NDT) controls are then carried out there in order to precisely assess the condition state. Following the results, a diagnosis is deduced and reparation procedure is potentially suggested [2]. In some cases, an additional step is carried out by use of models to plan the next inspection or repair.

While seemingly simple and effective, this method is limited by the faculty to visually detect pathologies, which is quite impossible in some cases like early reinforcing steel corrosion. It is moreover risky and out of budget to evaluate degradation all over the structure.

Increasing the use of Non-Destructive Techniques, widely developed during the last decade, allows to avoid these problems by measuring physical properties related to degradation mechanisms at high speed and low cost, without damaging the structure. Thus, it can easily replace or be complementary to the visual inspection step and lead to a more reliable inspection strategy, providing an optimal measurement grid. Indeed, while a coarse grid may be blind to degradation, a tight one can lead to unnecessary extra charge.

This last point is therefore a major research concern and has been recently investigated [2, 3, 4]. It is deeply related

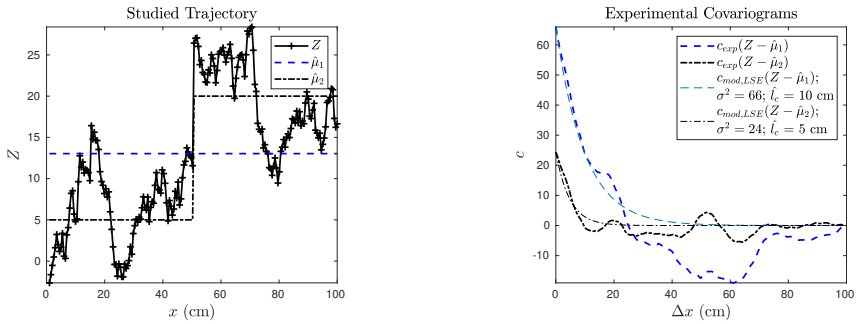

Figure 1: Experimental covariograms for different assessments of the mean : case of a non-stationary trajectory

to the spatial variability of the material properties, characterized, in case of stationarity, by a fluctuation parameter, also called correlation length (l_c), which can be computed through geostatistical analysis.

Nowadays, due to the lack of rich spatial studies on pathologies of concrete structures, there is no reliable correlation length database which can be used to determine optimal NDT-measurement grids. Hence there is a need to perform prior rapid NDT-measurements on a fine grid to assess correlation length [2].

Thanks to geostatistic tools, such as covariograms and semi-variograms [5, p. 58 – 68], and regression techniques, like Least-Square Estimation (LSE), evaluating correlation length seems trivial and authors usually assess it on raw measurements [3, 6, 7]

However, for a covariogram (or a semi-variogram) of a set of measurements $\boldsymbol{Z}$ to be meaningful, two major hypotheses on Z have to be checked : it has to be a realization of a (i) stationary and (ii) ergodic random field. If one of the hypotheses is not valid, interpretation based on variograms may not be relevant which is illustrated on Figure 1, with a non-stationary trajectory. We point out that straightforward interpretation may even be hazardous for risk analysis applications as they can lead to significantly underestimate probabilities of failure [8]

On Figure 1, Z is a realization of a Gaussian Random Field with piecewise-constant mean $\hat{\mu}_2 = \mu$ and exponential autocorrelation with correlation length of 10 cm. We note $\hat{\mu}_1$ the classic mean estimator. Thus, $Z - \hat{\mu}_1$ is non-stationary and non-ergodic whereas $Z - \hat{\mu}_2$ is both stationary and ergodic. Then, even if the (dashed) experimental covariogram of $Z - \hat{\mu}_1$ seems visually correct and suggests stationarity, geostatistical parameters assessments based on it are false : here, the variance and correlation length LSE are respectively three times and two times lower than the real values (5 cm instead of 10 cm, and 24 instead of 66)!

These conditions raise then a major issue, as most concrete structures are exposed to non-uniform environmental conditions, which can lead to non-stationarity of their physical properties. For example, concrete resistivity on marine bridges is more likely to be lower at sea level than on the desk, independently of reinforcing steel corrosion. Thus, it is needed to determine which parts of measurements are due to deterministic (and potentially non-uniform) trend and which parts come from stationary processes.

This requires then to assess piecewise-polynomial geostatistical mean and to test stationarity and ergodicity hypotheses.

This paper proposes a spatial variability assessment procedure, called SCAP-1D, which aims to be reliable and adapted to unidimensional piecewise-trend-stationary realizations of gaussian random fields, with limited numbers of measurements. It is also adapted to non-gaussian random fields coming from Box-Cox transformation, such as log-normal random fields.

After a definition of the studied model and the presentation of the procedure steps (part 2), we develop its theoretical aspects (part 3) and validate it with three different types of synthetic data (part 4), covering the range of its capabilities. An application to Half-Cell Potential (HCP) measurements made on a pier from the Île de Ré bridge illustrates its capacities on a practical study case (part 5).

2 PRESENTATION OF SCAP-1D

2.1 RANDOM FIELD MODELING

The aim of the procedure is to rigorously assess the geostatistical properties (correlation length and variance) of piecewise-trend-stationary random fields $\mathscr{Z}$, from which realizations, also called trajectories, are noted Z and piecewise-linear means are noted $\mu(\cdot)$. In practical, each realization is georeferenced and we focus on unidimensional piecewise-trend-stationary realizations of gaussian random fields. Indeed, gaussian model keeps methodology description simple while piecewise-trend-stationary assumption is versatile and sufficient for a lot of applications with few measurement points and non-monotonic variations.

Thus, any Z is georeferenced by the unidimentional vector

$\boldsymbol{x} = (x_1, \ldots, x_n)$ and can be written as

$$Z(\boldsymbol{x}) = \mu(\boldsymbol{x}) + \sigma G(\boldsymbol{R}(f_{cov}(\boldsymbol{x}, l_c))) \Leftrightarrow \boldsymbol{Z} = \boldsymbol{\mu} + \sigma \boldsymbol{G} \quad (1)$$

where (i) $\sigma\boldsymbol{G}$ is the random part of $\boldsymbol{Z}$, i.e a georeferenced realization of a gaussian random field (ii) $\boldsymbol{R}$ is the auto-correlation matrix of $\boldsymbol{G}$, (iii) f_{corr} is the auto-correlation function of $\boldsymbol{G}$, (iv) l_c is the correlation length which parametrizes f_{corr} , (v) and σ is the standard deviation of the random part, considered constant. For the sake of simplicity, we develop here the procedure considering isotropic geostatistical parameters σ^2 and l_c. However, this assumption can be strong as it supposes the parameters independent of both the random field mean and the environmental effects. We must therefore remain vigilant as it is not straightforward depending on the type of studied data, such as resistivity measurements in marine environment [9].

The three main hypotheses to test in the following procedure, in order to validate this model and, thus, the use of geostatistical assessment tools, are then : (i) the stationarity of $\boldsymbol{G}$, (ii) its ergodicity and (iii) its gaussianity. This last point means the normality of $\boldsymbol{J}$, defined as $\boldsymbol{G}$ uncorrelated.

We point out the procedure is applicable to other types of trajectories, provided that they come from a Box-Cox transformation of gaussian ones. However, this type of transformation supposes that data are strictly positive and may modify the noise nature (from multiplicative to additive for instance, in the case of log-Normal data with multiplicative noise) . Moreover, we recall that in this case, SCAP-1D assesses the geostatistical parameters of the transformation. It is then needed to use inverse transformation to get the parameters of the original trajectory.

2.2 SCAP-1D FLOWCHART

The main steps of SCAP-1D procedure are presented in the flowchart on Figure 2. Each one is detailed in the following theoretical parts

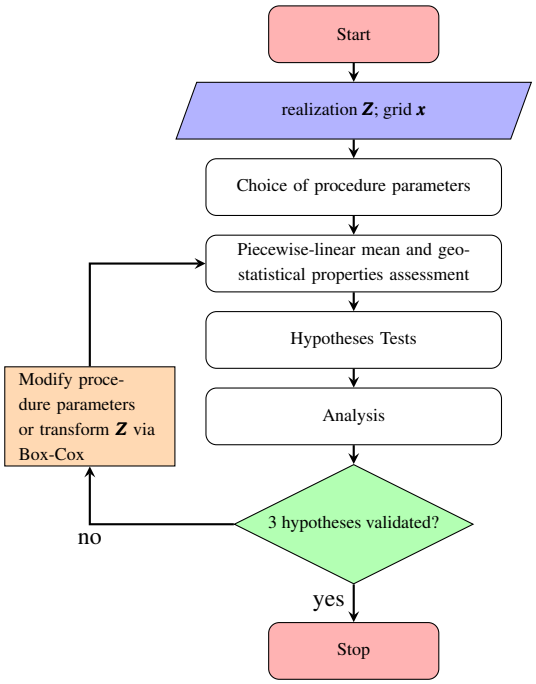

Figure 2: General flowchart of the procedure

3 THEORETICAL ASPECTS

In the following, $\boldsymbol{R}$ and $\boldsymbol{C}$ respectively refer to autocorrelation and auto-covariance matrix. The notation $\hat{\theta}$ refers to the estimation of the parameter θ.

3.1 PIECEWISE-POLYNOMIAL MEAN AND GEOSTATISTICAL PROPERTIES ASSESSMENT

The first step of the procedure aims to determine the deterministic trend of the studied trajectory, which is considered to be piecewise-linear with degree from zero to one. This model can indeed simply fit numerous physical and environmental phenomena, such as discontinuities of realization, or exposition parameter evolution. For example, Figure 3 illustrates the cases of piecewise-constant and piecewise-linear means observable on resistivity and corrosion potential measurements. These have been performed along the exterior face of a 0.4 x 0.86 x 9.84m^3 RC beam of the Montoir-de-Bretagne (France) coal terminal during the SVC2 (Spatial Variability of Chloride in Concrete) project [10].

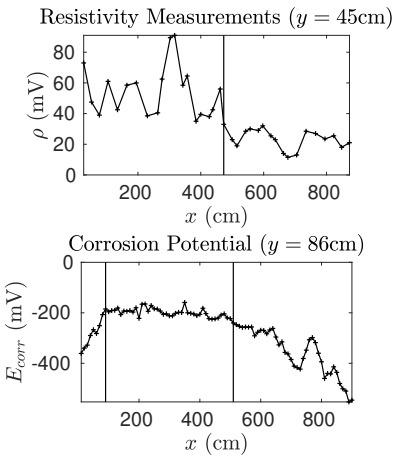

Figure 3: Choice of piecewise-linear mean model

It is therefore needed to detect changes of the mean, which can be mean and/or slope changes. This detection of geostatistical discontinuities, called edges hereafter, can be done visually or via statistical detection algorithms described afterwards in section 3.1.2. Then, it is possible to estimate the different continuous parts of the geostatistical mean with an iterative algorithm based on Maximum Likelihood Estima-

tion (MLE) and ruled by the error committed on geostatistical properties assessment. We outline the mechanics of this algorithm in the following and detail it in Appendix A.

3.1.1 Changepoints detection principle

Edge detection performed in the edges detection process of the procedure is done via hypothesis tests. In the general case of piecewise-linear mean, the null-hypothesis, noted H_0, suppose $\mu(\cdot)$ to be linear on the interval $[x_1;x_n]$ so that $\mu(x) = l_0.x + c_0$. In the case of H_0 being rejected, we note $x_r \in [x;x_n]$ the location of the changepoint detection. The hypothesis test can then be written as

$$\begin{cases} H_0 : \mu(x) = l_0.x + c_0 \\ \rightarrow \text{the mean is probably constant on } [x_1;x_n] \\ H_1 = \overline{H_0} : \exists r \in [1;n] \mid \\ \quad \mu(x)_{x\in[x_1,x_r]} = l_0.x + c_0 \quad \text{and} \\ \quad \mu(x)_{x\in[x_r,x_n]} = l_1.x + l_0.x_r + c_1 + c_0 \mid \\ \quad\quad c_0 \neq c_1 \quad \text{and/or} \quad l_0 \neq l_1 \\ \rightarrow \text{the mean is probably non constant on } [x_1;x_n] \end{cases} \tag{2}$$

3.1.2 Changepoints detection algorithm

Derived from time-series analysis, edges detection algorithms are not necessarily adapted to the study of NDT measurements trajectories, especially because of their limited number of measurements. That is why we reject Fourier and wavelet-analysis based methods [11, 12, 13]. There are, however, adaptable and performative ones, such as the Page-Hinkey algorithm (1954) [14, 15]. Presented by [16], this algorithm is used by [17] to detect transient states of random seas. It performs the hypothesis test described by eq.2 via a likelihood-ratio test which statistic D is written as

$$D = -2\log\left(\frac{L(\hat{r}_0)}{L(\hat{r}_1)}\right) \tag{3}$$

where $\hat{r}_0$ is the MLE of r under the null hypothesis whereas $\hat{r}_1$ is its MLE of r under the null hypothesis rejection. $L(\hat{r}_0)$ and $L(\hat{r}_1)$ are respectively $\hat{r}_0$ and $\hat{r}_1$ likelihoods.

We point out that, practically, $\hat{r}_0 = n$. Under the null hypothesis, D asymptotically follows a $\chi^2(3)$ probability density function. This means the limit value of the test statistic required to accept the null hypothesis under a fixed first species risk α is then the $(1-\alpha)$-quantile of $\chi^2(3)$.

In his paper, [16] presents a developed form of D adapted to step detection of the mean of uncorrelated gaussian trajectories. We modify it in eq.4 to take spatial correlation into account :

$$\begin{aligned} D = &\left[\log\left(|\hat{\boldsymbol{C}}_{H_0}|\right) + \left(\boldsymbol{Z} - \hat{\boldsymbol{\mu}}_{H_0}\right)' \cdot \hat{\boldsymbol{C}}_{H_0}^{-1} \cdot \left(\boldsymbol{Z} - \hat{\boldsymbol{\mu}}_{H_0}\right)\right] \\ &- \left[\log\left(|\hat{\boldsymbol{C}}_{H_1}|\right) + \left(\boldsymbol{Z} - \hat{\boldsymbol{\mu}}_{H_1}\right)' \cdot \hat{\boldsymbol{C}}_{H_1}^{-1} \cdot \left(\boldsymbol{Z} - \hat{\boldsymbol{\mu}}_{H_1}\right)\right] \end{aligned} \tag{4}$$

where $\boldsymbol{\mu}_{H_0}$ and $\boldsymbol{C}_{H_0}$ are the MLE of the mean and the estimation of the auto-covariance matrix of $\boldsymbol{Z}$ under the null hypothesis, whereas $\boldsymbol{\mu}_{H_1}$ and $\boldsymbol{C}_{H_1}$ are the MLE of the mean and the estimation of the auto-covariance matrix of $\boldsymbol{Z}$ under the null hypothesis rejection. The MLE of r under the null hypothesis rejection, needed to assess these last values, is computed through

$$\begin{aligned} \hat{r}_1 = &\underset{1\leq r\leq n}{\operatorname{argmin}}[\\ &\log\left(|\hat{\boldsymbol{C}}_{H1}(r)|\right) + \left(\boldsymbol{Z} - \hat{\boldsymbol{\mu}}_{H_1}(r)\right)' \cdot \hat{\boldsymbol{C}}_{H1}(r)^{-1} \cdot \left(\boldsymbol{Z} - \hat{\boldsymbol{\mu}}_{H_1}(r)\right) \\ &] \end{aligned} \tag{5}$$

The Page-Hinkley Algorithm is "online", which means it performs the hypothesis test (2) on growing samples of the trajectory, i.e piece-by-piece in a serial fashion, until it finds a changepoint. This way of computing geostatistical discontinuities is adapted to the study of spatial trajectories but requires numerous estimations of the mean and the auto-covariance matrix, which have to be as accurate as possible to determine "real" edges.

Consequently, a robust edges detection involving this algorithm cannot be done separately from the iterative process of mean, variance and correlation length assessment. The stationarity, ergodicity and gaussianity of $\boldsymbol{G}$ have to be validated as well for each iteration. It could be then a practicable solution to perform the whole spatial variability assessment procedure through this sole algorithm.

However, the precedent point currently implies one major issue : the current iterative process is already strongly time-consuming for medium-sized trajectories, as it is noticed in the numerical part. Another issue is the lack of numerical criterion to admit or reject ergodicity. This step is indeed currently done visually by looking at the experimental covariograms (see 4.1.2).

We propose then to not take into account spatial correlation during the automatic edges detection process, which however implies to firstly not consider the spatial variability of the trajectory. Nevertheless, its mean, variance and correlation length estimations which follow are performed in a strict geostatistical context. We show in the following that this does not significantly affects the robustness of the whole procedure as we here only aim to keep the locations of the discontinuities.

Thus, we use the Pruned Exact Linear Time (PELT) algorithm (2012) [18], which allows to determine exact statistical mean regression coefficients discontinuities, considering the whole trajectory. This "offline" algorithm is an improvement of the Optimal Partitioning one [19], which maximizes the likelihood of the edges locations, penalized by the number of discontinuities. Whereas the Optimal Partitioning algorithm is $o(n^2)$, the ability of the PELT one to delete impossible edges location while dividing the trajectory makes it

$o(n\log(n))$.

Once the edges are determined, $\boldsymbol{\mu}$ can be assessed by piecewise-spatial-regression. The whole methodology is described on Figure 4 and is detailed in the following sections.

3.1.3 Maximum-Likelihood Estimation of the mean

Since the unbiased estimator of the statistical mean which minimizes its variance is its MLE, we choose to use the MLE of the geostatistical mean to perform the piecewise regression.

Considering a gaussian trajectory $\boldsymbol{G}$ with a constant mean μ, it can be written as

$$\hat{\mu} = \frac{\boldsymbol{G}'\boldsymbol{R}^{-1}\mathbf{1}_n}{\mathbf{1}_n'\boldsymbol{R}^{-1}\mathbf{1}_n} \quad [4] \tag{6}$$

However, considering a piecewise-trend-stationary one, its georeferenced mean vector is $\boldsymbol{\mu} = \boldsymbol{A}\boldsymbol{\alpha}$, where $\boldsymbol{A}$ is the nodal piecewise-linear function matrix on the vector $\boldsymbol{x}$ of discrete positions and $\boldsymbol{\alpha}$ is the regression coefficients vector.

Example 1

Let $\boldsymbol{x} = (x_1, x_2, x_3, x_4, x_5)$. Let suppose $\mu(\cdot)$ is piecewise-linear so that

$$\begin{cases} \forall x \in [x_1, x_3], \mu(x) = l_0.x + c_0 \\ \forall x \in [x_3, x_5], \mu(x) = l_1(x - x_3) + c_1 \end{cases} \tag{7}$$

Then,

$$\boldsymbol{A} = \begin{pmatrix} 1 & x_1 & 0 & 0 \\ 1 & x_2 & 0 & 0 \\ 1 & x_3 & 0 & 0 \\ 0 & 0 & 1 & x_3 - x_3 \\ 0 & 0 & 1 & x_4 - x_3 \\ 0 & 0 & 1 & x_5 - x_3 \end{pmatrix} \quad \textit{and} \quad \boldsymbol{\alpha} = \begin{pmatrix} c_0 \\ l_0 \\ c_1 \\ l_1 \end{pmatrix}$$

The MLE of the mean is then

$$\hat{\boldsymbol{\mu}} = \boldsymbol{A}\boldsymbol{\alpha} \mid \boldsymbol{\alpha}' = \frac{\boldsymbol{Z}'\boldsymbol{R}^{-1}\boldsymbol{A}}{\boldsymbol{A}'\boldsymbol{R}^{-1}\boldsymbol{A}} \tag{8}$$

This means assessing $\boldsymbol{\mu}$ requires to assess both $\boldsymbol{A}$, which is done following the edges detection process, and $\boldsymbol{\alpha}$, which is to be done and implies the joint estimation of the correlation length of $\boldsymbol{G}$.

Thus, we develop an iterative assessment algorithm (Appendix A). Knowing the type of the auto-covariance function (i.e exponential, gaussian, Matérn, ...; see 4.6) and the nodal piecewise-linear function matrix, it provides estimations of $\boldsymbol{\mu}$, $\boldsymbol{G}$, σ^2 and l_c. The stop criterion is reached whenever the difference between two successive estimations of one geostatistical parameter is below an initially fixed tolerance. Therefore, this algorithm is adapted to nodal piecewise-polynomial function matrix.

Estimations are done via MLE, preferred to LSE. Indeed, although LSE is consistent (convergent) and allows to simply approach, in a visually effective way, the $\boldsymbol{G}$ covariogram, its estimators are not effective (with minimum variance), they are biased and it is difficult to assess their asymptotic laws, which are needed to compute their Confidence Regions (CR). It is still interesting to compute initial values through LSE, which is computationally-inexpensive (see Table 4), in order to fasten algorithm convergence, though.

On the contrary, MLE is consistent, asymptotically normal, and its effectiveness has been proven by [22] for gaussian vectors and by [23] for linear-trend-stationary gaussian vectors. Moreover, CR of MLE estimators $\hat{\theta}$ are easily determined by computing the Fischer Information Matrix I_1, as

$$\begin{aligned} CR_{\hat{\theta}} &= \left[CR_{min}(\hat{\theta}); CR_{max}(\hat{\theta})\right] \\ &= \left[\hat{\theta} - q_\alpha \frac{1}{\sqrt{I_1(\hat{\theta})}} \; ; \; \hat{\theta} + q_\alpha \frac{1}{\sqrt{I_1(\hat{\theta})}}\right] \end{aligned} \tag{9}$$

with q_α the α-quantile of the standard normal distribution. Following [4], we compute asymptotic CR so that only diagonal components of I_1 have then to be determined. Then, we have

$$I_1(\hat{\sigma}^2) = \frac{n}{2\hat{\sigma}^4} \tag{10}$$

$$I_1(\hat{l_c}) = \frac{1}{2}\mathrm{Tr}\left[\left(\boldsymbol{R}^{-1}\frac{\partial \boldsymbol{R}}{\partial \hat{l_c}}\right)^2\right] \tag{11}$$

$$I_1(\hat{\alpha_j}) = \frac{1}{\hat{\sigma}^2}\left([A_{ij}]_{i=1}^n\right)'\boldsymbol{R}^{-1}\left([A_{ij}]_{i=1}^n\right) \tag{12}$$

We henceforth get a robust estimation of $\boldsymbol{G}$, the gaussian random part of the studied trajectory (eq.1). We still need to test the normality, stationarity and ergodicity hypotheses, which validations are needed to confirm the choice of the auto-covariance function type, the mean and variance assessments, as well as the correlation length estimation.

3.2 HYPOTHESES TESTS

The second step of the procedure aims to test the three random field model hypotheses, the validity of which allows to consider assessments above as mathematically rigorous. On the one hand, stationarity and normality hypotheses tests are performed on $\hat{\boldsymbol{J}}$, below defined as $\hat{\boldsymbol{G}}$ uncorrelated. On the other hand, ergodicity is visually determined from the drawing of the experimental covariogram.

3.2.1 Normality tests

Let $\hat{\boldsymbol{J}}$ be defined as

$$\hat{\boldsymbol{J}} = \boldsymbol{Q}\hat{\boldsymbol{G}} \tag{13}$$

where $\boldsymbol{Q}$ is the lower triangular matrix obtained via Cholesky decomposition of the autocorrelation matrix $\boldsymbol{R}$ of $\hat{\boldsymbol{G}}$. Provided that $\hat{\boldsymbol{G}}$ is gaussian, $\hat{\boldsymbol{J}}$ is a vector of independent and identically distributed random variables. Then, testing the

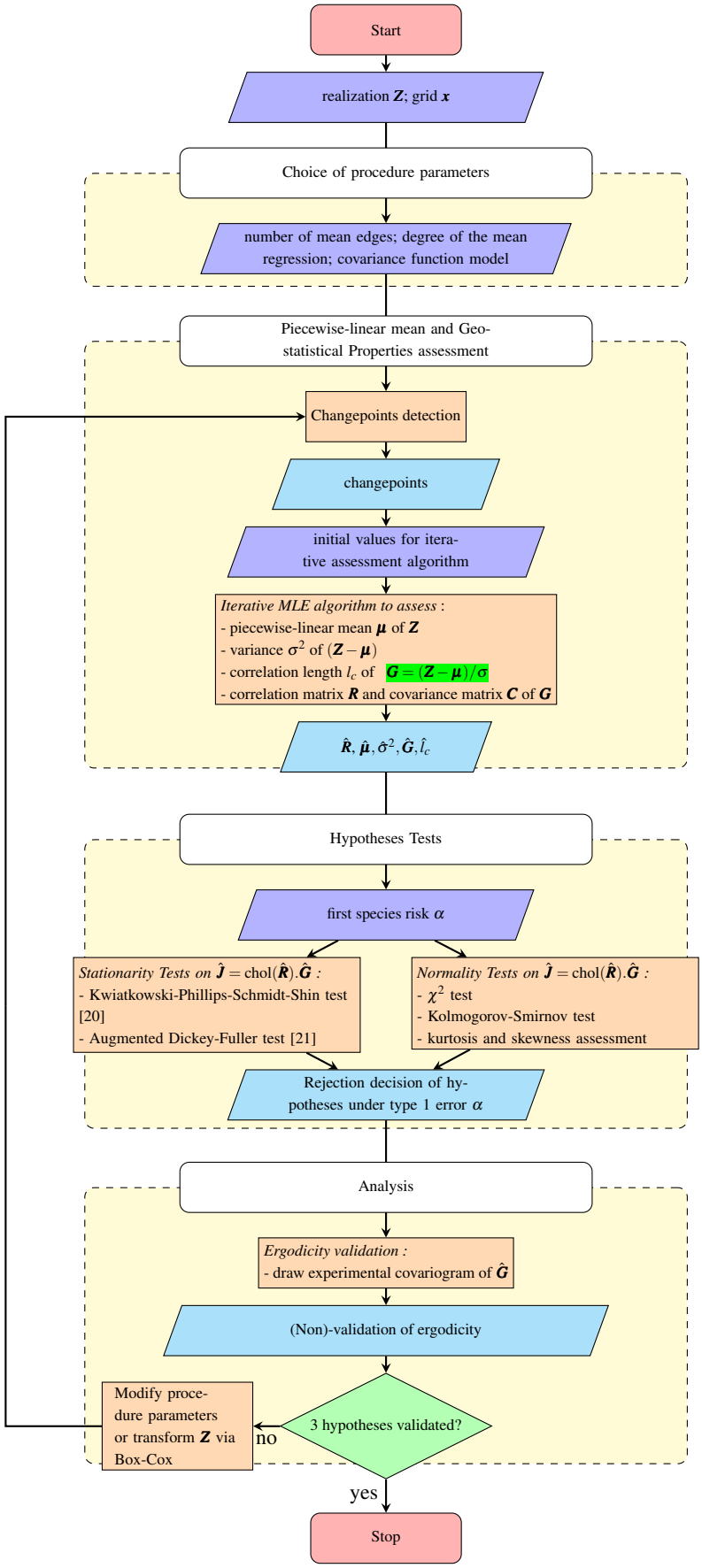

Figure 4: Detailed flowchart of the procedure

normality of $\hat{\boldsymbol{J}}$ equates to test $\hat{\boldsymbol{G}}$ gaussianity, on condition that estimations of geostatistical properties of $\hat{\boldsymbol{G}}$ are accurate.

The most popular normality tests are the Chi-squared (χ^2) goodness-of-fit test and the Kolmogorov-Smirnov (KS) test, where the null hypothesis is that the tested data comes from a normal distribution – for χ^2-test – or a standard normal distribution – for KS-test – . They are both applied to $\hat{\boldsymbol{J}}$ to improve the reliability of the procedure.

In the case where the choice of the initial Box-Cox transformation, i.e the type of probability distribution supposed for $\boldsymbol{Z}$, is not trivial after performing tests for different ones, the analysis can be completed with two additional steps. On the one hand, the likelihood of the distributions estimated parameters $L_f(\hat{\mu},\hat{\sigma}^2)$ can be evaluated and compared [24, p. 141]. The distribution which gives the maximum likelihood value shall then be retained. On the other hand, the skewness (third standardized moment, noted s) and kurtosis (fourth standardized moment, noted k) of $\hat{\boldsymbol{J}}$ can be assessed for these different cases. Indeed, if $\hat{\boldsymbol{J}}$ is normally distributed and noting $\hat{\mu}_J$ its mean estimation, we get

$$\hat{s} \underset{n\geq 3}{=} \frac{n^2}{(n-1)(n-2)} \frac{\frac{1}{n}\sum_{i=1}^{n}(\hat{J}_i-\hat{\mu}_J)^3}{\hat{\sigma}^3} \underset{n\to+\infty}{\longrightarrow} 0 \tag{14}$$

and

$$\hat{k} \underset{n\geq 4}{=} \frac{n^2(n+1)}{(n-1)(n-2)(n-3)} \frac{\frac{1}{n}\sum_{i=1}^{n}(\hat{J}_i-\hat{\mu}_J)^4}{\hat{\sigma}^4} - 3\frac{(n-1)^2}{(n-2)(n-3)} + 3 \underset{n\to+\infty}{\longrightarrow} 3 \tag{15}$$

The distribution which gives $\hat{s}$ closest to zero and $\hat{k}$ closest to three shall then be retained.

We advise to conclude from the first step results, more quantitative, and to use the second step ones to assess the need for new distributions tests.

3.2.2 Stationarity tests

Definition 1 *We recall that a random field $\mathscr{Z}$ is weakly stationary (or second order stationary, noted SOS) on a domain D if and only if (iff) its expected value is constant on D and its covariance exists and is an invariant translation function, i.e*

$$\begin{aligned} \forall x \in D, \quad \mathbb{E}[Z(x)] &= \mu \quad \text{(constant)} \\ Cov(Z(x_i),Z(x_j)) &= C(x_i - x_j) \end{aligned} \tag{16}$$

$C(\cdot)$ is the covariogram of $\mathscr{Z}$. We suppose here the second point is valid.

As the stationarity of a random field cannot be reliably evaluated through visual analysis of the experimental covariogram of a single realization (see Figure 1), we rely on statistical tests.

Two different approaches can be used to conclude about the stationarity of a stochastic process. The first is to test the null hypothesis of non-stationarity, whereas the second is to test the null hypothesis of stationarity. Although the difference may seem thin, as hypotheses tests only try to reject the null hypothesis with an α confidence level, it is of interest to perform tests with opposite null hypothesis, in order to confirm their result. This point has been discussed in [20]. Thus, we use both a stationarity and a non-stationarity test in the procedure.

These tests are both based on derived form of ARMA (AutoRegressive Moving Average) processes, which are general representations of stochastic series :

$$G(x) = \underbrace{\sum_{i=1}^{p}\beta_i G(x-i)}_{\text{AR(p) part}} + \varepsilon(x) + \underbrace{\sum_{i=1}^{q}\theta_i \varepsilon(x-i)}_{\text{MA(q) part}} \tag{17}$$

with $\varepsilon(x)$ independent and identically distributed (iid) error terms and β_i and θ_i parameters of the model.

KPSS-test the stationarity test developed by Kwiatkowsky, Phillips, Schmidt and Shin [20], noted KPSS in the following, is based on an ARMA process of order (1,1), meaning $p = 1$ and $q = 1$, with nuisance parameter $\beta_1 = 1$. This process is an alternative form of series composed by the sum of a constant ξ (which should be null in case of a centered trajectory), a random walk $r(x)$ and a stationary error $G_\varepsilon(x)$:

$$\begin{aligned} G(x) &= \beta G(x-1) + \varepsilon(x) + \theta\varepsilon(x-1) \\ &= \xi + r(x) + G_\varepsilon(x) \end{aligned} \tag{18}$$

with $r(x) = r(x-1) + u(x)$, so that $u(x)$ is iid. The hypothesis test is performed on θ and can be written as

$$\begin{cases} H_0 : \theta = -1; \lambda = \frac{\sigma_u^2}{\sigma_{G_\varepsilon}^2} = 0; \text{Var}(r(x)) = 0 \\ \quad \rightarrow \text{SOS cannot be rejected} \\ H_1 = \overline{H_0} : \theta \neq -1; \lambda = \frac{\sigma_u^2}{\sigma_{G_\varepsilon}^2} \neq 0; \text{Var}(r(x)) \neq 0 \\ \quad \rightarrow \text{SOS is rejected at 1-}\alpha\ \% \end{cases} \tag{19}$$

Let $S_x = \sum_{i=1}^{x} e_i$ be the partial sum process of the residuals, with $e_x = G(x) - \hat{\mu}_G$ the residual from the regression of G. The statistic used to formulate the decision rule of the test (also called test statistic) is then either $LM = \sum_{x=1}^{N} S_x^2/\hat{\sigma}_e^2$, or $LM^c = N^{-2}\sum_{x=1}^{N} S_x^2/s^2(l)$, depending on the residuals autocorrelation.

Indeed, while LM is based on iid residuals, LM^c takes their dependence over space into account with an estimation of the long-run variance. This term is defined by KPSS as $\sigma^2 = \lim_{N\to\infty} N^{-1}E[S_N^2]$ and its consistent estimator writes

$$s^2(l) = T^{-1}\sum_{x=1}^{N} e_x^2 + 2T^{-1}\sum_{s=1}^{l} w(s,l)\sum_{x=s+l}^{N} e_x e_{x-s} \tag{20}$$

with l the number of lags, which represent the autocorrelation range in terms of measuring points, and $w(s,l) = \left(1 - \frac{s}{l+1}\right)$ a weighting function.

At first sight, as $\hat{\boldsymbol{G}}$ is meant to have an autocorrelation structure. KPSS-test should then be performed with LM^c statistic. However, the weighting function is arbitrary fixed to ensure estimator consistency. Thus, s^2 does not take into account the evaluation of autocorrelation coefficients performed during the previous step of the procedure. Moreover, [25] and [26] point out that, for highly autocorrelated series, the probability of false rejection of the null hypothesis for stationarity tests is dramatically high whereas the probability of correct rejection it is radically low.

We also point out that, on the contrary, KPSS-test shows good results with non-correlated series.

These remarks push ourselves into using KPSS-test with LM statistic on $\hat{\boldsymbol{J}}$. By doing so, the inability to reject the null hypothesis would suppose both the stationarity of G and the accuracy of the mean, variance and correlation length assessment.

DF-test the non-stationarity test developed by Dickey and Füller [21], noted DF in the following, is based on an ARMA process of order (1,0).

The hypothesis test is performed on β and can be written as

$$\begin{cases} H_0 : \beta = 1 \\ \quad \rightarrow \text{presence of a unit root} \\ \quad \rightarrow \text{non-SOS cannot be rejected} \\ H_1 = \overline{H_0} : |\beta| < 1 \\ \quad \rightarrow \text{absence of a unit root} \\ \quad \rightarrow \text{non-SOS is rejected at 1-}\alpha\ \% \end{cases} \tag{21}$$

The test statistic is $t = \frac{\hat{\beta}-1}{\sigma}$, with $\hat{\beta}$ the LSE of β and σ its standard error.

There is an "augmented" version of this test, called Augmented Dickey-Füller test, which takes into account AR(p) processes and so consider autocorrelation. However, following previous remarks, we opt for the use of DF-test on $\hat{\boldsymbol{J}}$.

3.2.3 Ergodicity

Definition 2 *We recall that a random field $\mathscr{Z}$ is ergodic iff its standardized moments can be computed by spatial average, from only one trajectory. In the case where $\mathscr{Z}$ is SOS, $\mathscr{Z}$ is ergodic in L^2 iff*

$$\lim_{D \to \mathbb{R}^n} \frac{1}{|D|} \int_D Z(x)dx = \mu \quad \Leftrightarrow \quad \lim_{h=|x_i-x_j| \to |D|} C(h) = 0 \tag{22}$$

As soon as the stationarity hypothesis is validated, checking ergodicity is trivial. Indeed, it only requires to draw the empirical covariogram of $\hat{\boldsymbol{G}}$ and to check it tends to zero as the distance between two measurement points approaches the size of the studied area. For some trajectories, a doubt can remain about ergodicity. In this case, typically when the covariogram tends to zero at the boundaries of the domain with no oscillation around the abscissa axis, we recommend precaution and to consider them non-ergodic. However, this does not systematically mean the procedure fails as other random fields and/or auto-covariance models can be considered.

We also point out that, if we study several trajectories supposed to be realizations of the same random field, ergodicity can be more reliably checked by comparison, under certain criteria, of both the trajectories mean estimations and the experimental covariograms [27, p. 7]. However, in the case of limited data, such an approach is unlikely.

3.3 STEP BY STEP ANALYSIS

Once normality and stationarity tests are performed, their results are analyzed together in order to conclude about the validity of the three main hypotheses on G, the random part of the trajectory.

Stationarity hypothesis is considered as valid only if the null hypothesis of KPSS-test cannot be rejected and the null of DF-test is rejected. In the opposite case, G is considered non-stationary, while in the other cases, there is a doubt and we cannot conclude with certainty from the tests results.

Similarly, gaussianity hypothesis is considered as valid if the null hypothesis of χ^2-test and KS-test cannot be rejected, and false in the opposite case. However, in the other case, G may be nonetheless considered as gaussian if the null of KS-test cannot be rejected and both the skewness and kurtosis are respectively close to zero and three. Indeed, KS-test is more robust than the χ^2-test as it considers a continuous distribution. Table 1 sums up this two first analysis steps.

Once stationarity and gaussianity are validated, there is still to check the ergodicity (3.2.3).

Once all of these three hypotheses are validated, we can conclude that the model choice and the geostatistical properties assessments made during both the first and the second step of the procedure are correct, including the correlation length estimation.

If at least one of the hypotheses cannot be validated, we cannot affirm that the whole trajectory follows the model previously chosen with assessed geostatistical parameters. The main reasons to this failure can be, in no particular order, the presence of aberrant data, the possibility that either the correlation length or the variance is not constant over the studied area, the wrong detection of mean edges and the construction of the model. In the latter case, several parameters can be wrong : (i) the regression degree, (ii) the distribution model, i.e the choice of the initial Box-Cox transformation (see 3.2.1), (iii) the number of mean edges, or (iv) the choice of the auto-covariance function. Each of these issues should be checked.

Table 1: Hypothesis-tests results analysis

Normality test results on J		Gaussianity of G	Stationarity test results on J		Stationarity of G
χ^2	KS-test		KPSS-test	ADF-test	
FALSE	FALSE	YES	FALSE	FALSE	NO
FALSE	TRUE	NO	FALSE	TRUE	YES
TRUE	FALSE	YES	TRUE	FALSE	NO
TRUE	TRUE	NO	TRUE	TRUE	NO

This last remark points out that, due to the numerous parameters influencing the procedure, knowledge of the phenomenon described by studied trajectory and its global physical characteristics is necessary to efficiently use it.

In the following, we apply the procedure to synthetic data with total control over the model parameters. Tests will be performed with type I error of 5%, *i.e* with 5% probability of incorrect rejection of a true null hypothesis.

4 NUMERICAL VALIDATION

In order to demonstrate abilities of the procedure, we test it on unidimensional synthetic data, so that we utterly control the model parameters. Results are given in explicit tables and illustrated by four-parts figures (such as Figure 6) which show (i) the studied trajectory $\boldsymbol{Z}$, its mean MLE $\hat{\boldsymbol{\mu}}_{MLE}$ and its real mean $\boldsymbol{\mu}$ (ii) the experimental covariogram deduced from mean estimation, the real experimental covariogram and the modelled covariogram derived from the correlation length l_c assessment (iii) the -2.log-likelihood of l_c plotted from the two mean estimations (iv) the cumulative density functions of the uncorrelated standardized trajectories deduced from the two mean estimations, compared to the standard normal one.

For the sake of clarity, the procedure execution time and the methods allowing its improvement are discussed afterwards in section 4.4.

4.1 CASE OF A CONSTANT MEAN

4.1.1 Trajectories simulation

As a first step, the procedure is tested on stationary trajectories. Realizations of a unique gaussian random field *GRF*, which main parameter are presented in Table 2, are generated using the embedding circulant matrix (ECM) method. This technique allows to exactly simulate stationary gaussian processes [28]. Procedure is then applied to the trajectories in order to check good assessment of the model parameters. The length of the support of the trajectories and the number of "measurements" in each one of them is given in Table 2.

The constant mean is chosen to be sufficiently far from zero to assess estimation error without getting extremely high values. The variance is set so that $\sigma \simeq \mu$. This is an unfavorable numerical case for the following cases of mean step and bilinear mean. The correlation length is chosen both in order to avoid numerical problems and to get a realistic ratio l_c/L [3, 6].

We point out that ergodicity is not granted by ECM. Thus, we choose to simulate twenty trajectories, noted $[t_1, \ldots, t_{20}]$ in order to get a sufficient number of stationary, gaussian and ergodic ones.

4.1.2 Ergodicity hypothesis validation

Experimental auto-covariances are drawn considering the real value of the mean, in order to discriminate the non-ergodic trajectories, as illustrated by Figure 5.

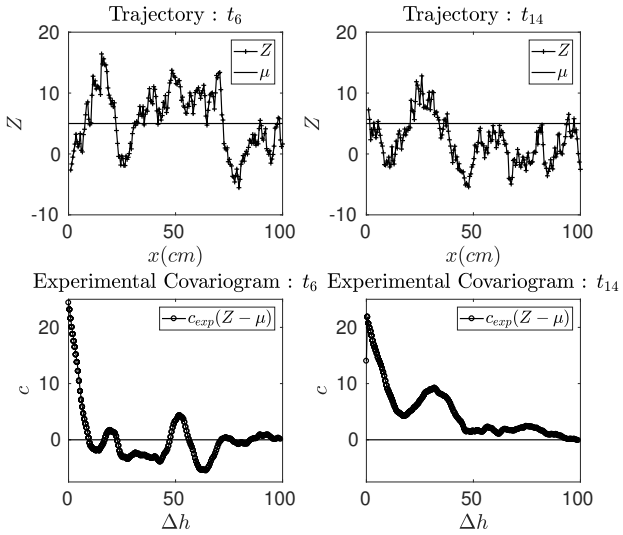

Figure 5: Experimental covariograms of t_6 and t_{14}

Here, t_6 is considered ergodic as its covariogram oscillates around zero from 75% of the length of the support. On the contrary, the covariogram of t_{14} only reach zero for $x = 100$, which is not sufficient to admit ergodicity. t_{14} is then rejected and will not be submitted to the procedure.

Following this discrimination process, only 11 out of the 20 stationary and gaussian simulated trajectories are considered ergodic. Procedure is then applied to them.

4.1.3 Procedure validation

Table 3 presents the results of the procedure applied to the 11 stationary-gaussian-ergodic trajectories, with the auto-

Table 2: *GRF* and trajectory parameters

Parameter	Property	Value
mean	constant	$\mu = 5$
variance	constant	$\sigma^2 = 25$
auto-covariance function	Matérn model	$f_{cov}(h) = \sigma^2 \frac{2^{1-\nu}}{\Gamma(\nu)} \left(\sqrt{2\nu}\frac{h}{l_c}\right)^{\nu} K_\nu \left(\sqrt{2\nu}\frac{h}{l_c}\right)$ $(\star)$
auto-covariance regularity parameter	-	$\nu = 0.5$
correlation length	constant	$l_c = 10$
support size	-	$L = 100$
number of "measurement points"	uniform grid	$n = 200$

$(\star)$ **Γ : gamma function, K_ν : modified Bessel function of the second kind**

covariance parameter ν assumed to be known.

Following test results interpretations given by Table 1, all the 11 ergodic trajectories are found to be stationary and gaussian, so that assessments of both their geostatistical parameters and their confidence region (*CR*) are mathematically valid. Estimation errors and coefficients of variation (CoV) are then computed for each trajectory, as well as their mean.

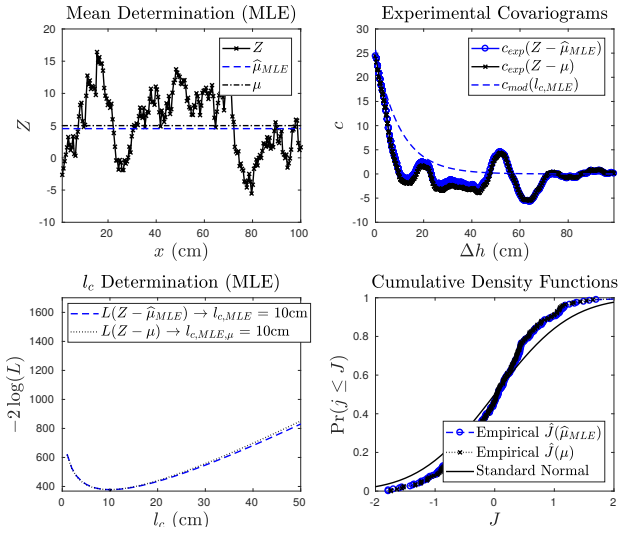

Figure 6: Illustration of the procedure calculations for t_6

At first sight, the procedure seems accurate : (i) the estimation error on correlation length varies from 1,02% (t_6, with procedure calculations illustrated on Figure 6) to 57,19% (t_7) with only three trajectories above 30% (t_2, t_7, t_{13}) and an average of 24,33%, (ii) the mean one lies between 1,96% (t_9) and 31,23% (t_{17}) with an average of 14,97%, and (iii) the variance is assessed with an error from 1,81% (t_9) to 55,71% (t_7) with two trajectories above 30% (t_7, t_{13}) and an average of 22,57%. We also point out that the CoV of the mean and the variance are quite low (around 10%) thanks to the high sample size. The correlation length CoV is higher with an average of 35,97%, which is mostly due to a relatively high value. Thus, estimation error rarely exceeds 30% and coefficients of variation are quite low, especially for the variance and the correlation length.

In order to confirm this analysis and to demonstrate the interest of the recursive procedure, we perform the classic parameters estimation scheme on the studied trajectories. The mean and the variance are computed neglecting spatial variation and the correlation length is obtained via LSE on experimental covariogram. Results are given in Table 4.

The error bounds on the mean estimation are quite similar to the procedure results with a minimum of 0,15% (t_1), a maximum of 32,83% (t_17) and an average of 14,58%. Likewise, the variance is assessed with an error from 2,98% (t_{11}) to 54,60% (t_7) with an average of 21,55%, and 2 trajectories above 30% (t_7 and t_{13}). However, the estimation error on the correlation length is significantly higher, from 6.41% (t_{18}) to 65,20% (t_7) with an average of 36,25%, which is 12 points over the procedure average, and seven trajectories above 30% (t_6, t_7, t_{10}, t_{11}, t_{13}, t_{17}, t_{20}).

The CoV of the variance is still 10% as the sample size did not change. On the contrary, the CoV of the mean is frankly mitigated (minus 29 points). However, this is due to the non-inclusion of the spatial variability hypothesis in estimators, which has just been shown to result in significant errors on the estimation of the correlation length.

Thus, the mathematically rigorous procedure developed in this paper is more accurate than the classical parameters estimation scheme, especially for the correlation length assessment.

4.2 CASE OF A MEAN STEP

As a second step, procedure is tested on piecewise constant mean, i.e piecewise stationary, trajectories. This case represents for instance corrosion on vertical profile of steel wharves [29]. Analyzing results of the first validation step, we note error estimation on parameters is minimal for the t_6 trajectory, which is therefore chosen to be our "base" trajectory. Mean steps of 10 different intensities $s = k.\sigma$ are then applied to t_6 at the middle of the support length on $x = 50,5$ (n=101), in order to establish performance range of the procedure in this general case. Such phenomenon can be faced when structures presents discontinuities (cracks, isolation joints). The generated trajectories are then noted $t_{6.sk}$.

Table 5 presents results and Figure 7 illustrates application

Table 3: Procedure results : case of a constant mean

Procedure Results												
t	1	2	6	7	9	10	11	13	17	18	20	
$\hat{\mu}$	5,65	4,57	4,53	4,28	5,10	5,83	3,66	5,90	6,56	4,53	4,10	
$CR_{min}(\hat{\mu})$	2,20	-0,72	0,44	2,44	0,96	2,52	0,09	3,46	3,61	1,22	-0,47	
$CR_{max}(\hat{\mu})$	9,11	9,86	8,62	6,12	9,24	9,15	7,22	8,35	9,51	7,83	8,66	
$\hat{\sigma}$	4,62	5,67	5,07	3,33	4,95	4,42	4,89	3,70	4,32	4,31	5,35	
$\hat{\sigma}^2$	21,31	32,18	25,68	11,07	24,55	19,54	23,94	13,72	18,70	18,62	28,66	
$CR_{min}(\hat{\sigma}^2)$	17,13	25,87	20,64	8,90	19,74	15,71	19,25	11,03	15,04	14,97	23,05	
$CR_{max}(\hat{\sigma}^2)$	25,48	38,48	30,71	13,24	29,36	23,37	28,63	16,41	22,37	22,27	34,28	
$\hat{l}_c$	8,46	14,48	10,10	4,28	10,98	8,49	7,94	6,32	6,81	8,94	11,54	
$CR_{min}(\hat{l}_c)$	6,75	11,59	8,07	3,39	8,77	6,77	6,33	5,03	5,43	7,13	9,22	
$CR_{max}(\hat{l}_c)$	10,17	17,38	12,14	5,17	13,19	10,20	9,55	7,61	8,20	10,74	13,85	
$h(\chi^2-\text{test})$	FALSE	FALSE	FALSE	FALSE	FALSE	FALSE	FALSE	FALSE	FALSE	FALSE	FALSE	
$h(\text{KS}-\text{test})$	FALSE	FALSE	FALSE	FALSE	FALSE	FALSE	FALSE	FALSE	FALSE	FALSE	FALSE	
k	2,74	3,37	4,49	3,31	3,21	2,79	3,53	2,93	3,26	2,89	3,19	
s	0,08	0,30	0,33	-0,02	-0,05	0,10	-0,01	0,02	0,04	-0,09	-0,15	
$h(\text{KPSS}-\text{test})$	FALSE	FALSE	FALSE	FALSE	FALSE	FALSE	FALSE	FALSE	FALSE	FALSE	FALSE	
$h(\text{ADF}-\text{test})$	TRUE	TRUE	TRUE	TRUE	TRUE	TRUE	TRUE	TRUE	TRUE	TRUE	TRUE	
Ergodicity	TRUE	TRUE	TRUE	TRUE	TRUE	TRUE	TRUE	TRUE	TRUE	TRUE	TRUE	
Results Analysis												Average
error μ	13,09%	8,63%	9,33%	14,38%	1,96%	16,62%	26,90%	18,10%	31,23%	9,47%	18,08%	14,97%
error σ^2	14,77%	28,71%	2,71%	55,71%	1,81%	21,85%	4,25%	45,13%	25,19%	25,53%	14,66%	22,57%
error l_c	15,40%	44,84%	1,02%	57,19%	9,79%	15,15%	20,58%	36,80%	31,87%	10,64%	15,36%	24,33%
CoV $\hat{\mu}$	31,19%	59,08%	46,02%	21,94%	41,41%	29,00%	49,78%	21,11%	22,93%	37,28%	56,83%	35,97%
CoV $\hat{\sigma}^2$	10,00%	10,00%	10,00%	10,00%	10,00%	10,00%	10,00%	10,00%	10,00%	10,00%	10,00%	10,00%
CoV $\hat{l}_c$	10,32%	10,20%	10,27%	10,61%	10,25%	10,32%	10,34%	10,42%	10,39%	10,31%	10,24%	10,34%
t_{calc} (s)	793,65	1042,53	951,69	531,22	944,64	831,11	726,60	707,22	658,93	803,53	924,31	799,11

Table 4: classical parameters estimation scheme results

Procedure Resuts												
t	1	2	6	7	9	10	11	13	17	18	20	
$\hat{\mu}$	4,99	4,52	5,53	4,12	5,31	6,08	3,71	5,42	6,64	3,94	4,68	
$CR_{min}(\hat{\mu})$	4,35	3,73	4,85	3,65	4,60	5,45	3,01	4,94	6,02	3,34	3,94	
$CR_{max}(\hat{\mu})$	5,63	5,30	6,22	4,58	6,01	6,71	4,41	5,90	7,26	4,54	5,43	
$\hat{\sigma}$	4,63	5,66	4,94	3,37	5,10	4,54	5,07	3,46	4,47	4,34	5,38	
$\hat{\sigma}^2$	21,39	32,05	24,39	11,35	26,03	20,57	25,74	11,98	19,96	18,82	28,90	
$CR_{min}(\hat{\sigma}^2)$	17,20	25,77	19,61	9,13	20,93	16,54	20,70	9,63	16,05	15,13	23,24	
$CR_{max}(\hat{\sigma}^2)$	25,59	38,34	29,17	13,58	31,13	24,60	30,79	14,32	23,87	22,50	34,57	
$\hat{l}_c$	11,12	8,62	4,45	3,48	11,09	4,94	6,45	5,36	3,94	10,64	5,74	
Results Analysis												Average
error μ	0,15%	9,64%	10,61%	17,64%	6,13%	21,65%	25,83%	8,41%	32,83%	21,17%	6,35%	14,58%
error σ^2	14,43%	28,22%	2,43%	54,60%	4,11%	17,72%	2,98%	52,10%	20,17%	24,73%	15,62%	21,55%
error l_c	11,24%	13,84%	55,54%	65,20%	10,89%	50,58%	35,46%	46,39%	60,59%	6,41%	42,59%	36,25%
CoV $\hat{\mu}$	6,55%	8,86%	6,31%	5,79%	6,80%	5,27%	9,67%	4,51%	4,76%	7,78%	8,12%	6,77%
CoV $\hat{\sigma}^2$	10,00%	10,00%	10,00%	10,00%	10,00%	10,00%	10,00%	10,00%	10,00%	10,00%	10,00%	10,00%
t_{calc} (s)	0,23	0,09	0,08	0,06	0,08	0,06	0,06	0,06	0,06	0,06	0,06	0,08

Note : $CR_{min}(\hat{l}_c)$, $CR_{max}(\hat{l}_c)$ and CoV $\hat{l}_c$ cannot be simply evaluated as the Least-Square Estimator of $\hat{l}_c$ is not its Maximum-Likelihood Estimator (see eq.9).

of the procedure with $s = 10$ ($k = 2$). Mean steps are sorted in three ranges in order to ease analysis : (i) range 1 (k from 0,1 to 1,5), (ii) range 2 (k from 1,5 to 3), (iii) range 3 (k from 3 to 10). Highlighted cells indicate issues during the SCAP-1D procedure.

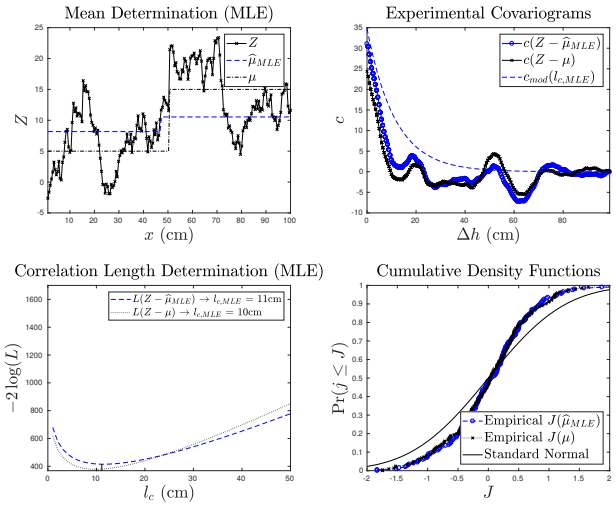

Figure 7: Illustration of the procedure calculations for $t_{6.s2}$

Indeed, trajectories with mean steps from range 1 ($t_{6.s01}$ to $t_{6.s1,5}$), once centered, are considered either non-stationary ($t_{6.s01}$,$t_{6.s025}$) or non-gaussian ($t_{6.s05}$ to $t_{6.s1,5}$). These rejections are either due to wrong step detection, with an error from 43,56% ($t_{6.s01}$,$t_{6.s025}$) to 98,02% ($t_{6.s05}$, $t_{6.s1}$), and/or to wrong mean assessment, as each trajectory gets an error above 30% on the first mean level (α_1) and/or the second mean level (α_2) estimation (except $t_{6.s05}$). Thus, the SCAP-1D procedure is not adapted to the assessment of mean steps in the first range. However, we highlight that in this step range, it does not give false results as hypotheses rejections indicate that geostatistical estimations cannot be considered as mathematically valid.

On the contrary, range 2 steps ($t_{6.s5}$) may induce wrong estimations : whereas estimation errors are non-negligible and even quite high for trajectory $t_6.s2$, with 63,36% for the first mean level, 29,75% for the second mean level and 39,13% for the variance, the centered trajectory is considered stationary, gaussian and ergodic, which implies the user to (wrongly) consider estimations are accurate. Thus, the SCAP-1D procedure can be treacherous in the second step range.

Unlike range 1 and range 2 ones, range 3 steps are very well detected with accurate estimations of both mean steps locations and geostatistical parameters : the error on the step detection, the first mean level, the variance and the correlation length are constant (from $t_{6.s3}$ to $t_{6.s10}$) and respectively are 0%, 6,86%, 2,05% and 0,35%. The error on the second mean level varies from 2,89% ($t_{6.s3}$) to 1,05% ($t_{6.s10}$). This variability comes from the increasing value of α_2, whereas variance stays constant, which induces a decreasing of its estimator CoV, from 7,20% to 2,57%.

Following this analysis, the procedure appears adapted to trajectories with mean steps above two times the standard deviation of the stationary field, defining its operating range as $s \geq 2.\sigma$. Even if this step size is significant in classic statistical analysis, it is here an interesting result. Indeed, as illustrated by Figure 7, such a gap may not be obvious at first sight while working with autocorrelated fields. We however point out that, at this range, estimation error on parameters may be significant. It is therefore required to analyze results with physical background.

4.3 CASE OF A BILINEAR MEAN

As a final step, procedure is tested on piecewise trend-stationary trajectories. The base trajectory is still t_6. Six new trajectories are generated by adding a bilinear mean with a first null slope (α_2), a changepoint at the middle of the support on $x = 50,5$ ($n = 101$) and a second slope of 6 different intensities $\alpha_3 = k.\sigma/L$, with k from 2 (trajectory $t_{6.b2}$) to 40 (trajectory $t_{6.b40}$). This allows to establish performance range of the procedure in this general case. Such phenomenon can be faced with edge effects or environmental conditions variation [30]. Generated trajectories are noted $t_{6,bk}$, k being the slope index.

Table 6 presents results and Figures 8 and 9 illustrate application of the procedure respectively on $t_{6,b30}$ and $t_{6,b10}$. Slope steps are sorted in three ranges in order to ease analysis : (i) range 1 (k from 2 to 5), (ii) range 2 (k from 10 to 20), (iii) range 3 (k from 30 to 40). Highlighted cells indicate issues during the SCAP-1D procedure.

General remarks

Before refining the analysis, it is of interest to point out that the mean intercept (α_1) estimation error is significant for each trajectory, from 39,12% ($t_{s6;b2}$) to 118,92% ($t_{s6;b20}$). This can be explained by the fact that the variance is equal to the first mean level. However, it is not a real issue as this parameter only estimate one point (the first one) of the mean and because the first mean slope (α_2) is generally well-assessed, with an error between 9,74% ($t_{s6;b2}$) to 33,84% ($t_{s6;b10}$).

Refined analysis

Giving the results, it appears that range 1 slope steps ($t_{6.b2}$, $t_{6.b5}$) may induce wrong assessment of slope change location : while SCAP-1D procedure does not reject neither stationarity nor gaussianity, nor ergodicity hypotheses, the estimation errors on slope change location are significant, from 43,56% $t_{6.b2}$ to 98,02% $t_{6.b5}$. However, geostatistical parameters are well estimated : the variance estimation error is about 30% in both cases, as well as the correlation length one. This numerical phenomenon is due to the low values of the slope

Table 5: Procedure results : case of a mean step

Procedure Results										
t	6.s10	6.s5	6.s4	6.s3	6.s2	6.s1,5	6.s1	6.s05	6.s025	6.s01
k	10	5	4	3	2	1,5	1	0,5	0,25	0,1
x step detect	50,50	50,50	50,50	50,50	47,00	46,50	100,00	100,00	72,50	72,50
$\hat{\alpha}_1$	4,66	4,66	4,66	4,66	8,17	6,64	6,98	5,80	6,59	6,28
$CR_{min}(\hat{\alpha}_1)$	1,92	1,92	1,92	1,92	5,08	3,78	2,58	1,78	4,19	3,91
$CR_{max}(\hat{\alpha}_1)$	7,40	7,40	7,40	7,40	11,25	9,49	11,39	9,83	9,00	8,65
$\hat{\alpha}_2$	54,42	29,42	24,42	19,42	10,54	9,84	6,98	5,80	2,60	2,18
$CR_{min}(\hat{\alpha}_2)$	51,68	26,68	21,68	16,68	7,48	7,03	NaN	NaN	-0,12	-0,52
$CR_{max}(\hat{\alpha}_2)$	57,16	32,16	27,16	22,16	13,59	12,65	NaN	NaN	5,32	4,87
$\hat{\sigma}$	5,05	5,05	5,05	5,05	5,90	5,12	5,34	5,04	4,41	4,32
$\hat{\sigma}^2$	25,51	25,51	25,51	25,51	34,78	26,21	28,48	25,40	19,48	18,70
$CR_{min}(\hat{\sigma}^2)$	20,51	20,51	20,51	20,51	27,97	21,07	22,90	20,42	15,67	15,04
$CR_{max}(\hat{\sigma}^2)$	30,51	30,51	30,51	30,51	41,60	31,35	34,07	30,38	23,30	22,37
$\hat{l}_c$	10,04	10,04	10,04	10,04	11,47	9,36	10,69	9,87	7,81	7,50
$CR_{min}(\hat{l}_c)$	8,01	8,01	8,01	8,01	9,17	7,47	8,54	7,88	6,22	5,98
$CR_{max}(\hat{l}_c)$	12,06	12,06	12,06	12,06	13,77	11,25	12,84	11,86	9,39	9,03
$h(\chi^2-\text{test})$	FALSE	FALSE	FALSE	FALSE	FALSE	FALSE	FALSE	FALSE	FALSE	FALSE
$h(\text{KS}-\text{test})$	FALSE	FALSE	FALSE	FALSE	FALSE	FALSE	FALSE	FALSE	TRUE	TRUE
k	4,47	4,47	4,47	4,47	8,34	5,62	4,36	4,29	4,54	4,62
s	0,33	0,33	0,33	0,33	1,06	0,65	0,35	0,29	0,26	0,28
$h(\text{KPSS}-\text{test})$	FALSE	FALSE	FALSE	FALSE	FALSE	TRUE	TRUE	TRUE	FALSE	FALSE
$h(\text{ADF}-\text{test})$	TRUE	TRUE	TRUE	TRUE	TRUE	TRUE	TRUE	TRUE	TRUE	TRUE
ergodicity	TRUE	TRUE	TRUE	TRUE	TRUE	TRUE	TRUE	TRUE	TRUE	TRUE
Results Analysis										
error x step detect	0,00%	0,00%	0,00%	0,00%	6,93%	7,92%	98,02%	98,02%	43,56%	43,56%
error α_1	6,86%	6,86%	6,86%	6,86%	63,36%	32,75%	39,68%	16,07%	31,85%	25,51%
error α_2	1,05%	1,93%	2,31%	2,89%	29,75%	21,28%	30,16%	22,62%	58,35%	60,45%
error σ^2	2,05%	2,05%	2,05%	2,05%	39,13%	4,84%	13,94%	1,61%	22,06%	25,18%
error l_c	0,35%	0,35%	0,35%	0,35%	14,69%	6,40%	6,92%	1,32%	21,92%	24,95%
cov $\hat{\alpha}_1$	30,03%	30,03%	30,03%	30,03%	19,28%	21,96%	32,21%	35,41%	18,63%	19,27%
cov $\hat{\alpha}_2$	2,57%	4,75%	5,73%	7,20%	14,78%	14,57%	NaN	NaN	53,33%	63,26%
cov $\hat{\sigma}^2$	10,00%	10,00%	10,00%	10,00%	10,00%	10,00%	10,00%	10,00%	10,00%	10,00%
cov $\hat{l}_c$	10,27%	10,27%	10,27%	10,27%	10,24%	10,29%	10,26%	10,28%	10,35%	10,36%
t_{calc} (s)	949,70	952,25	1 006,24	1 009,89	1 168,63	985,60	1 030,77	977,68	771,65	751,86

steps, which imply modified and original trajectories to be then quite similar. Thus, the procedure is not adapted to the assessment of slope steps in the first range.

We also note that trajectories with slope steps from range 2 ($t_{6.b10}$, $t_{6.b20}$), once centered, are considered non-gaussian ($t_{6.b20}$) and/or non-ergodic (both). These rejections are either due to wrong step detection, with an error around 60%, and/or to wrong mean assessment : both of them get an error above 40% on the second slope (α_3) assessment. Thus, the SCAP-1D procedure is not adapted to the assessment of slope steps in the second range. However, we highlight that, in this range, it does not give false results as hypotheses rejections indicate that geostatistical estimations cannot be considered as mathematically valid.

However, unlike range 1 and range 2 ones, range 3 steps ($t_{6.b30}$, $t_{6.b40}$) are very well detected by the algorithm, with estimation errors of 1,98% ($t_{6.b30}$) and 0,99% ($t_{6.b40}$). Moreover, variance and correlation length estimations on the two centered trajectories are also accurate, with errors between 28,14% and 29,88%, while the second slope is assessed with less than 15% error for both.

Following this analysis, the procedure appears adapted to trajectories with slope steps above 1.5, i.e $30\sigma/L$. However, the error on mean and parameters estimations is limited but higher than in case of a piecewise constant mean. Thus, for potential multilinear cases, the different slopes have to be quite pronounced in order to use this procedure and have confidence in estimations.

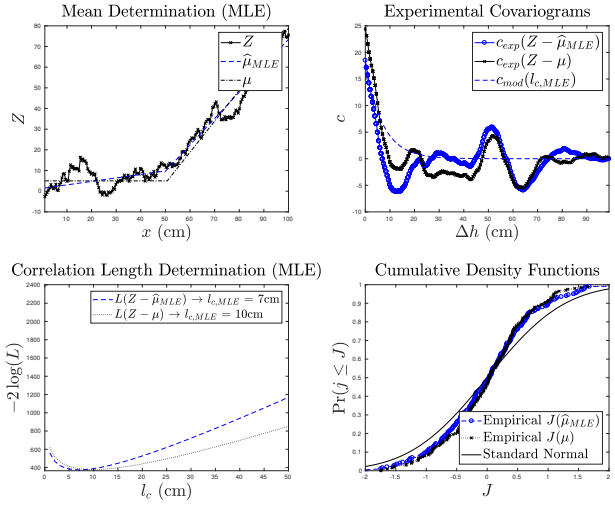

Figure 8: Illustration of the procedure calculations for $t_{6.b30}$

4.4 COMPUTATIONAL TIME REDUCTION

The main drawback of the procedure is its computational time (Tables 3,5, 6) which is about 10.000 times longer than the LSE method one (Table 4). We expose here two simple ways to reduce this factor to 2500 while conserving the same estimators precision. These are applied on the t_6 trajectory

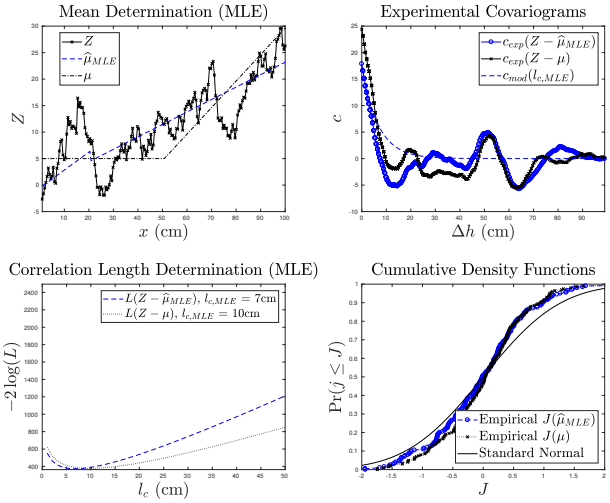

Figure 9: Illustration of the procedure calculations for $t_{6.b10}$

(Table 3, Figure 6) and results are given on Table 7.

The first one is to determine the initial correlation length l_{c0} (algorithm in Appendix A) with LSE on experimental covariogram. Indeed, if no *a priori* values of the correlation length are known, this allows to shrink the distance between this initial value, normally arbitrary fixed, and the MLE of l_c. Applied to t_6 (noted $t_6.ctr1$ for computational time reduction), this leads to a reduction factor of 1,5.

A second one is to increase the tolerance on geostatistical parameters evaluation (algorithm in Appendix A). Indeed, the opposite log-likelihood function ℓ of GRF is regular and presents a unique minimum in the studied interval $[0, L]$ and the expected accuracy on l_c is of the order of 1cm. Attention should however be paid to the slope of ℓ in the neighborhood of its minimum : a wide minimum zone requests short tolerance to get accurate minimization whereas large tolerance is sufficient for a sharp one.

This method is applied to t_6 (noted $t_6.ctr2$ below). Initial tolerance of $1e^{-5}$cm is reduced to $1e^{-2}$cm, which leads to a reduction factor of 2 with comparable estimation errors.

Combining these two methods (noted $t_6.ctr3$), the total computational time of the procedure applied to t_6 is divided by 4 without any loss of precision and accuracy.

4.5 EFFECTS OF THE DOMAIN CHOICE AND SIZE

Another important parameter affecting the procedure's effectiveness is the choice of both the location and the size L of the studied domain D.

Indeed, if mean edges are next to the boundaries of D, there are risks that they cannot be precisely detected by the PELT algorithm. This implies wrong parameters assessments and reject of the main hypotheses. This phenomenon is highlighted on Table 8 and Figures 11 and 12 : both trajectories t6.b40 and t6.s3 are truncated, first on $x_q = 7/8L$, then on $x_q = 5/8L$, so that mean edge, located on x_{100} approaches the

Table 6: Procedure results : case of a bilinear mean

Procedure Results						
t	6.b40	6.b30	6.b20	6.b10	6.b5	6.b2
k	40	30	20	10	5	2
α_3 (2nd slope)	2	1,5	1	0,5	0,25	0,1
x edge detect	50	49,5	22	20,5	100	72,5
$\hat{\alpha}_1$ ($\hat{\mu}(x=0)$)	1,25	1,38	-0,95	-0,55	2,83	3,04
$CR_{min}(\hat{\alpha}_1)$	-1,25	-1,13	-3,86	-3,30	-0,15	0,85
$CR_{max}(\hat{\alpha}_1)$	3,75	3,88	1,96	2,20	5,81	5,24
$\hat{\alpha}_2$ (1st slope)	0,18	0,17	0,17	0,34	0,11	0,10
$CR_{min}(\hat{\alpha}_2)$	0,12	0,11	0,03	0,19	0,06	0,06
$CR_{max}(\hat{\alpha}_2)$	0,24	0,23	0,31	0,48	0,16	0,13
$\hat{\alpha}_3$ (2nd slope)	1,79	1,28	0,59	0,23	NaN	0,02
$CR_{min}(\hat{\alpha}_3)$	1,75	1,24	0,52	0,19	NaN	-0,01
$CR_{max}(\hat{\alpha}_3)$	1,83	1,32	0,65	0,28	NaN	0,05
$\hat{\sigma}$	4,23	4,24	5,26	4,15	4,28	3,95
$\hat{\sigma}^2$	17,91	17,97	27,66	17,20	18,29	15,62
$CR_{min}(\hat{\sigma}^2)$	14,40	14,44	22,24	13,83	14,70	12,56
$CR_{max}(\hat{\sigma}^2)$	21,42	21,49	33,08	20,58	21,87	18,68
$\hat{l}_c$	7,02	7,01	11,03	6,76	7,16	6,26
$CR_{min}(\hat{l}_c)$	5,59	5,58	8,81	5,38	5,70	4,98
$CR_{max}(\hat{l}_c)$	8,45	8,44	13,25	8,13	8,62	7,53
$h(\chi^2-\text{test})$	FALSE	FALSE	TRUE	FALSE	FALSE	FALSE
$h(\text{KS}-\text{test})$	FALSE	FALSE	FALSE	FALSE	FALSE	FALSE
k	5,73	5,74	5,27	5,54	5,24	5,49
s	0,65	0,66	0,55	0,62	0,58	0,61
$h(\text{KPSS}-\text{test})$	FALSE	FALSE	FALSE	FALSE	FALSE	FALSE
$h(\text{ADF}-\text{test})$	TRUE	TRUE	TRUE	TRUE	TRUE	TRUE
ergodicity	TRUE	TRUE	FALSE	FALSE	TRUE	TRUE
Results Analysis						
error x edge detect	0,99%	1,98%	56,44%	59,41%	98,02%	43,56%
error α_1	74,98%	72,43%	118,92%	111,02%	43,38%	39,12%
error α_2	17,97%	16,82%	17,15%	33,84%	10,73%	9,74%
error α_3	10,38%	14,96%	41,48%	53,02%	NaN	78,64%
error σ^2	28,37%	28,14%	10,62%	31,19%	26,85%	37,51%
error l_c	29,77%	29,88%	10,30%	32,44%	28,41%	37,44%
cov $\hat{\alpha}_1$	101,79%	92,71%	156,96%	254,66%	53,71%	36,75%
cov $\hat{\alpha}_2$	16,41%	17,76%	41,02%	21,99%	23,56%	19,56%
cov $\hat{\alpha}_3$	1,13%	1,59%	5,58%	9,77%	NaN	79,09%
cov $\hat{\sigma}^2$	10,00%	10,00%	10,00%	10,00%	10,00%	10,00%
cov $\hat{l}_c$	10,38%	10,38%	10,25%	10,40%	10,38%	10,43%
t_{calc} (s)	718,41	721,54	1 131,44	717,66	668,36	689,01

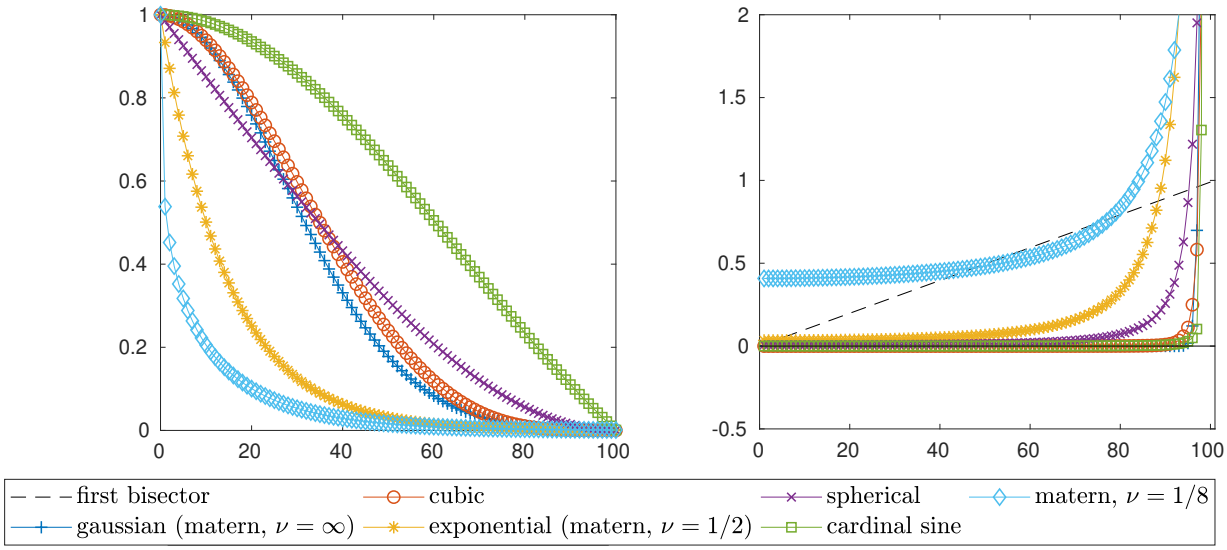

Figure 10: correlograms and eigenvalues of popular auto-covariance models

right boundary of the domain. This results in sub-trajectories t6.b40.q150, t6.b40.q125, t6.s3.q125 and t6.s3.q125, which are prior checked for ergodicity, considering their real mean values.

Whereas t6.b40 parameters are well assessed by the procedure (best results of Table 6), both t6.b40.q150 and t6.b40.q125 give inoperable results as either normality or ergodicity hypothesis is not valid, due to error on edge detection. On the contrary, t6.s3.q150 and t6.s3.q125 continue to give accurate estimations of the geostatistical parameters.

This leads to the interpretation that piecewise-trend-stationary trajectories are much more sensitive to the distance between potential edges and the domain boundaries than piecewise-stationary ones. Then, *a priori* knowledge about the potential mean edges is an asset to fix the studied domain boundaries. Practically, this issue can also be faced by truncating boundary measurements. Indeed, when on-site inspections are performed on whole structure elements, measurements next to boundaries are often affected by side effects and material heterogeneity. The procedure hypothesis of stationarity of geostatistical parameters is then not satisfied in these areas.

Moreover, if $l_c \simeq L$ or $l_c > L$, there is a great risk that measured trajectory will not be ergodic, by definition of the covariogram and l_c. Thus, provided l_c and σ are constant along L, the greater the domain, the likelier the ergodicity hypothesis [24, p. 92]. Then, *a priori* knowledge about the researched correlation length is a strong asset to fix the size of the domain. As an example, [31] shows that correlation length of surface chloride content on wharves RC beams can vary by up to four times depending on their wind exposition (sheltered or exposed). Thus, the domain needed to assess it on similar wind-exposed elements should *a priori* be significantly larger than for wind-sheltered ones .

4.6 EFFECTS AND CHOICE OF AUTO-COVARIANCE MODEL

The last choice which could influence the accuracy and the efficiency of the procedure is the auto-covariance model, which influences the mean and geostatistical parameters likelihood expression, i.e their MLE. However, [23] proves that under certain conditions of regularity (namely the absolute summability of the auto-covariance eigenvalues), the Maximum Likelihood Estimation is asymptotically normal, which means its accuracy is independent from the auto-covariance model. Practically, these conditions are fulfilled by Matérn models with $\nu \geq 0.5$, and cover most of the other popular models. This is illustrated on Figure 10), where it is clear that cubic, spherical, gaussian, exponential and cardinal sine auto-covariance eigenvalues are absolutely summable, whereas those of Matérn model with $\nu = 1/8$ are above the first bisector.

Thus, there is only few restrictions on the choice of auto-covariance function. Practically, its selection is based on the shape of the experimental covariogram or semivariogram of studied data. If a doubt remains, model comparison criteria such as Bayesian Information Criterion (BIC) or Akaike Inkormation Criterion (AIC) can be computed after the procedure to select the best model [32].

Table 7: Computational Time Reduction : effects on $t6$

Procedures Results				
t	6	6.ctr1	6.ctr2	6.ctr3
tolerance	1,00E-05	1,00E-05	1,00E-02	1,00E-02
l_{c0} type	arbitrary	LSE	arbitrary	LSE
l_{c0} value	25,00	4,70	25,00	4,70
$\hat{\alpha}$	4,53	4,53	4,52	4,55
$CR_{min}(\hat{\alpha})$	0,44	0,44	0,36	0,52
$CR_{max}(\hat{\alpha})$	8,62	8,62	8,67	8,57
$\hat{\sigma}$	5,07	5,07	5,11	5,02
$\hat{\sigma}^2$	25,68	25,67	26,14	25,24
$CR_{min}(\hat{\sigma}^2)$	20,64	20,64	21,02	20,29
$CR_{max}(\hat{\sigma}^2)$	30,71	30,71	31,26	30,18
$\hat{lc}$	10,10	10,10	10,28	9,93
$CR_{min}(\hat{lc})$	8,07	8,07	8,21	7,93
$CR_{max}(\hat{lc})$	12,14	12,13	12,35	11,93
$h(\chi^2-\text{test})$	FALSE	FALSE	FALSE	FALSE
$h(\text{KS}-\text{test})$	FALSE	FALSE	FALSE	FALSE
k	4,49	4,49	4,49	4,49
s	0,33	0,33	0,33	0,33
$h(\text{KPSS}-\text{test})$	FALSE	FALSE	FALSE	FALSE
$h(\text{ADF}-\text{test})$	TRUE	TRUE	TRUE	TRUE
ergodicity	TRUE	TRUE	TRUE	TRUE
Results Analysis				
error α	9,33%	9,33%	9,65%	9,02%
error σ^2	2,71%	2,70%	4,55%	0,95%
error l_c	1,02%	1,01%	2,84%	0,72%
cov α	46,02%	46,01%	46,94%	45,14%
cov σ^2	10,00%	10,00%	10,00%	10,00%
cov l_c	10,27%	10,27%	10,27%	10,28%
t_{calc} (s)	951,69	648,95	449,10	219,51
t_{calc} reduction factor		1,47	2,12	4,34

Table 8: Effect of the mean edge location : application on $t6.b40$ and $t6.s3$

Procedure Results							
t	6.b40	6.b40.q150	6.b40.q125	t	6.s3	6.s3.q150	6.s3.q125
q (trunc t)	-	150	125	q (trunc t)	-	150	125
α_3 (2nd slope)	2	2	2	k	3	3	3
x edge detect	100	97	44	x edge detect	101	101	101
$\hat{\alpha}_1$ ($\hat{\mu}(x=0)$)	1,25	0,98	-1,57	$\hat{\alpha}_1$	4,66	5,40	6,31
$CR_{min}(\hat{\alpha}_1)$	-1,25	-1,63	-4,56	$CR_{min}(\hat{\alpha}_1)$	1,92	2,59	3,62
$CR_{max}(\hat{\alpha}_1)$	3,75	3,58	1,42	$CR_{max}(\hat{\alpha}_1)$	7,40	8,21	8,99
$\hat{\alpha}_2$ (1st slope)	0,18	0,20	0,25	$\hat{\alpha}_2$	19,42	20,37	21,59
$CR_{min}(\hat{\alpha}_2)$	0,12	0,14	0,11	$CR_{min}(\hat{\alpha}_2)$	16,68	17,39	18,65
$CR_{max}(\hat{\alpha}_2)$	0,24	0,26	0,39	$CR_{max}(\hat{\alpha}_2)$	22,16	23,35	24,54
$\hat{\alpha}_3$ (2nd slope)	1,79	1,51	0,68				
$CR_{min}(\hat{\alpha}_3)$	1,75	1,46	0,57				
$CR_{max}(\hat{\alpha}_3)$	1,83	1,57	0,78				
$\hat{\sigma}$	4,23	4,37	5,97	$\hat{\sigma}$	5,05	5,07	4,80
$\hat{\sigma}^2$	17,91	19,14	35,59	$\hat{\sigma}^2$	25,51	25,66	23,09
$CR_{min}(\hat{\sigma}^2)$	14,40	14,81	26,77	$CR_{min}(\hat{\sigma}^2)$	20,51	19,86	17,36
$CR_{max}(\hat{\sigma}^2)$	21,42	23,47	44,41	$CR_{max}(\hat{\sigma}^2)$	30,51	31,47	28,81
$\hat{l}_c$	7,02	6,88	13,94	$\hat{l}_c$	10,04	9,25	9,02
$CR_{min}(\hat{l}_c)$	5,59	5,26	10,41	$CR_{min}(\hat{l}_c)$	8,01	7,09	6,72
$CR_{max}(\hat{l}_c)$	8,45	8,50	17,48	$CR_{max}(\hat{l}_c)$	12,06	11,40	11,33
$h(\chi^2-\text{test})$	FALSE	FALSE	FALSE	$h(\chi^2-\text{test})$	FALSE	FALSE	FALSE
$h(\text{KS}-\text{test})$	FALSE	FALSE	FALSE	$h(\text{KS}-\text{test})$	FALSE	FALSE	FALSE
k	5,73	4,81	5,42	k	4,47	4,54	5,35
s	0,65	0,61	0,69	s	0,33	0,34	0,47
$h(\text{KPSS}-\text{test})$	FALSE	TRUE	TRUE	$h(\text{KPSS}-\text{test})$	FALSE	FALSE	FALSE
$h(\text{ADF}-\text{test})$	TRUE	TRUE	TRUE	$h(\text{ADF}-\text{test})$	TRUE	TRUE	TRUE
ergodicity	TRUE	TRUE	FALSE	ergodicity	TRUE	TRUE	TRUE
Results Analysis							
error x edge detect	0,99%	3,96%	56,44%	error x step detect	0,00%	0,00%	0,00%
error α_1	74,98%	80,49%	131,36%	error α_1	6,86%	8,03%	26,16%
error α_2	17,97%	20,15%	25,17%	error α_2	2,89%	1,84%	7,96%
error α_3	10,38%	24,28%	66,18%				
error σ^2	28,37%	23,44%	42,36%	error σ^2	2,05%	2,66%	7,65%
error l_c	29,77%	31,20%	39,44%	error l_c	0,35%	7,54%	9,76%
cov $\hat{\alpha}_1$	101,79%	136,07%	97,35%	cov $\hat{\alpha}_1$	30,03%	30,81%	29,41%
cov $\hat{\alpha}_2$	16,41%	15,74%	28,35%	cov $\hat{\alpha}_2$	7,20%	7,46%	6,95%
cov $\hat{\alpha}_3$	1,13%	1,76%	8,02%				
cov $\hat{\sigma}^2$	10,00%	11,55%	12,65%	cov $\hat{\sigma}^2$	10,00%	11,55%	12,65%
cov $\hat{l}_c$	10,38%	12,01%	12,93%	cov $\hat{l}_c$	10,27%	11,90%	13,05%
t_{calc}(s)	425,47	214,72	347,91	t_{calc}(s)	659,53	369,55	246,69

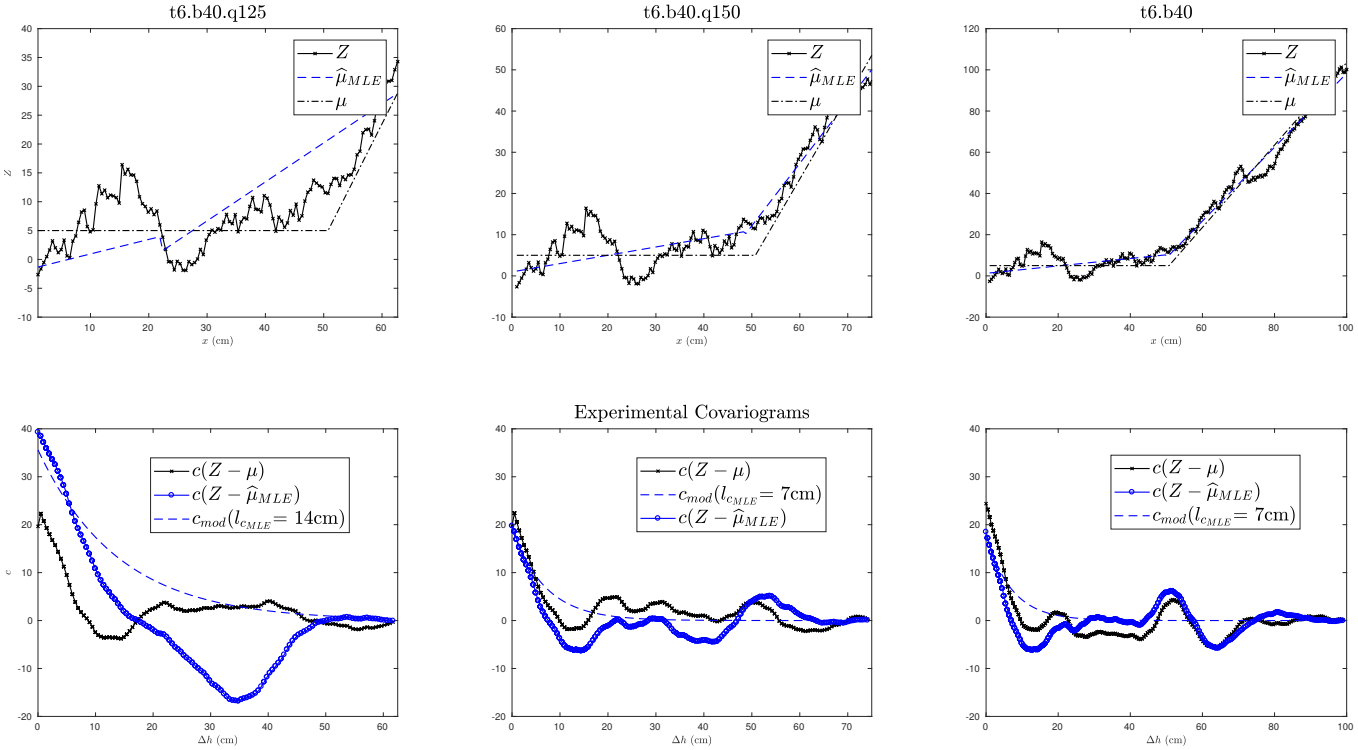

Figure 11: Reduction of the distance edge - *D* boundaries : application to t6.b40

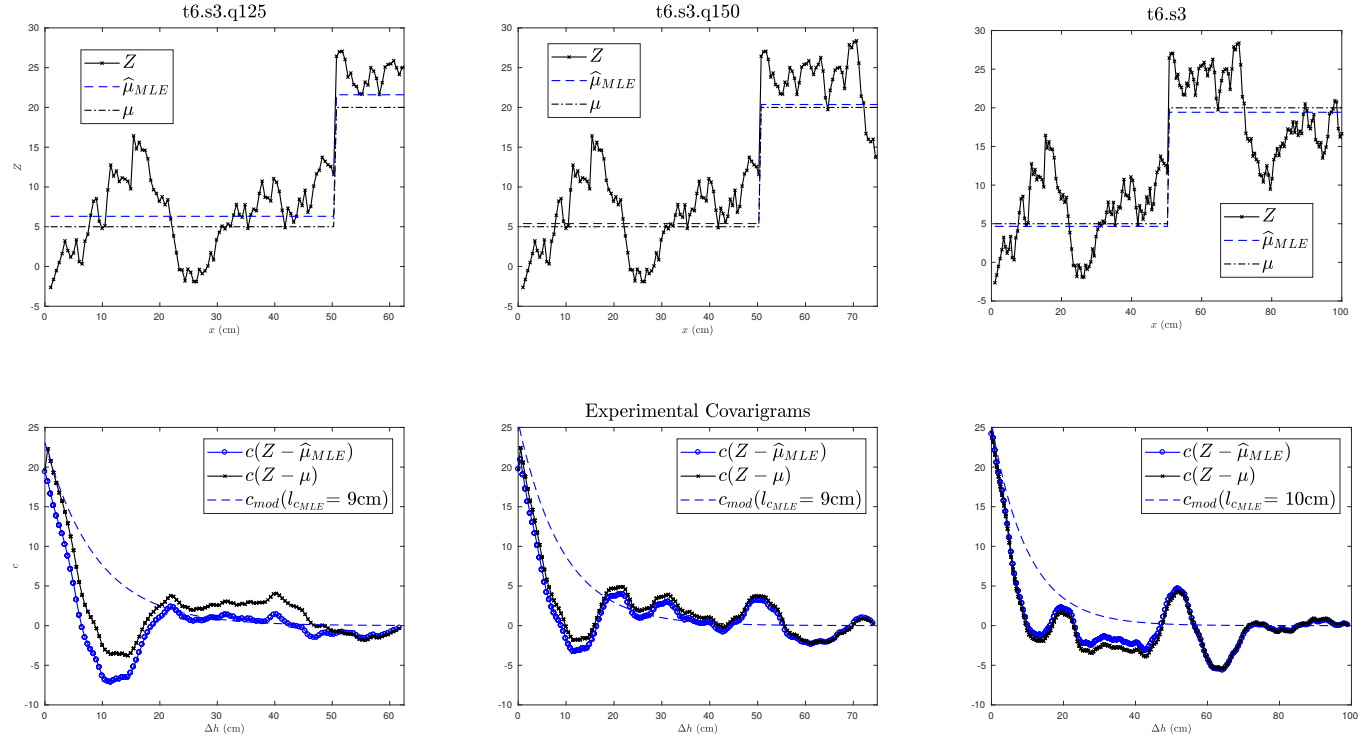

Figure 12: Reduction of the distance edge - *D* boundaries : application to t6.s3

5 EXPERIMENTAL VALIDATION ON A CASE STUDY

In this section, we test the SCAP-1D procedure with real data in the two cases of piecewise-constant and piecewise-linear mean.

5.1 THEORETICAL PREAMBLE

In preamble to this study, we shall recall that, contrary to the simple model used to present the SCAP-1D procedure, most experimental data are noisy. This noise and its prevalence in the signal can be simply visualized in case of stationarity by drawing the experimental semi-variogram of the data and checking for nugget effect [5, 33].

Usually, authors get rid of it by operating moving average on data [34]. However, we show in the following that this operation can affect the spatial variability properties of the signal (see Figure 13c).

Thus, in order to make SCAP-1D applicable on most real data sets, we shall transform the "development" model (Equation 1) to take additive white noise into account, so that we write

$$Z(\boldsymbol{x}) = \boldsymbol{A}(\boldsymbol{x})\boldsymbol{\alpha} + \sigma.G(\boldsymbol{R}(f_{cov}(\boldsymbol{x}, l_c))) + \tau.B(\mathbf{1}_n) \qquad (23)$$

with $B \sim \mathcal{N}(0,1)$. Then, the auto-covariance matrix $\boldsymbol{C}$ of $\boldsymbol{Z} - \boldsymbol{A}.\boldsymbol{\alpha}$ equates $\sigma.\boldsymbol{R} + \tau.\mathbf{1}_n$.

This model evolution has no impact on the general procedure algorithm and only induces modifications on estimators, presented in the updated iterative MLE algorithm in appendix B. The Fisher matrix is also modified but can be easily computed numerically. Eventually, the hypotheses test shall be performed on the uncorrelated trajectory $\boldsymbol{J}$, redefined as

$$\boldsymbol{J} = \boldsymbol{Q}(\boldsymbol{Z} - \boldsymbol{A}.\hat{\boldsymbol{\alpha}}) \qquad (24)$$

where Q is the lower triangular matrix obtained via Cholesky decomposition of C.

5.2 PRESENTATION OF THE STRUCTURE AND MEASUREMENTS

The studied structure is the Île de Ré bridge (France), built in 1987, which connects the Island of Ré to the mainland (Figure 13a). This RC bridge has been recently inspected by L. Bourreau during his PhD thesis [35] as part of the DéCoF-Ré project (Decision Corrosion Reliability on the Île de Ré Bridge), led by IFSTTAR. This study aimed to diagnose the piers corrosion state and to give decision help about scheduling and placement of future diagnostic operations. NDT inspections were carried out on 3-meters high and 1.85-meters wide wind-sheltered and wind-exposed faces (respectively FC and FG, Figure 13b) of 15 piers, during 4 seasons. They resulted in a huge database of Half-Cell Potential (HCP) and Electrical Resistivity (ER) measurements. This allowed, combined with SDT measurements, to bring out two fully healthy piers (noted PG and PN).

On one hand, the HCP measurement grid is very tight, with respectively 5 cm and 2 cm spacings on horizontal and vertical rebars. This results in 36-points horizontal trajectories and and 151-points vertical ones. On the other hand, the ER grid is much coarser with a mesh size about 20 cm. This results in 10-points horizontal trajectories and 15-points vertical ones. Moreover, [9] showed that the ER variance depends on the square of ER mean, which increases along the vertical.

Thus, in order to get meaningful assessments and to meet the hypothesis of constant variance and correlation length (made in the SCAP1D procedure), we focus on HCP data on healthy piers G and N in the following study.

Table 9: Boundaries between 2 zones for HCP data for the four seasons [36]

Boundaries between zones : (origin at +3.95 m CD)	High and Median (m)	Median and Low (m)
Winter	1.69 - 1.94	0.67 - 0.88
Spring	1.69 - 1.94	0.67 - 0.88
Summer	1.94 - 2.17	0.67 - 0.88
Autumn	1.94 - 2.17	0.88 - 1.07

5.3 CASE OF A MEAN STEP

Firstly, we validate the procedure in the experimental case of a mean step for three similar trajectories. In order to give the most meaningful comparison between the parameters assessments, we select two trajectories of the same pier face and measured the same day. Moreover, we focus on horizontal trajectories as vertical ones have piecewise-linear drift : this corresponds to different corrosion zones (tidal, splash and atmospheric zones), as RC corrosion behaves differently depending on chloride concentration and oxygen amount. They have been assessed by [36] and are defined on Table 9 .

Choice of test trajectories

Browsing horizontal HCP data measured in Automn, we find evidence of local mean step on the top of the atmospheric zone of Pier G Face C, at abscissa x=110 – 120 cm. This is illustrated on Figures 14a and 14b, were we draw the data cartography and the three related trajectories, noted H1, H2 and H3 (respectively measured at ordinates 2.98 m, 2.82 m and 2.58 m).

This step is not due to coating variability as there is no correlation structure between coating and HCP measurements in this zone, as we show on Figure 14c. However, it may be justified by the fluted shape of piers which implies different sun exposition time along the horizontal and thus drying variability (see Figure 13a). Indeed, while this phenomenon

(a) The Île de Ré bridge

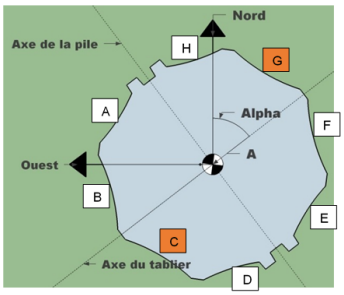

(b) Pier cross-sectional view

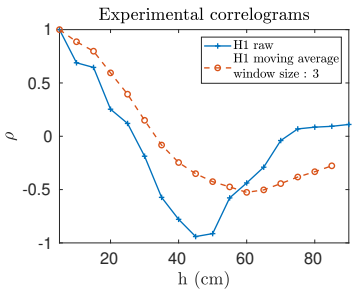

(c) Impact of moving average on spatial variability

Figure 13: Studied structure

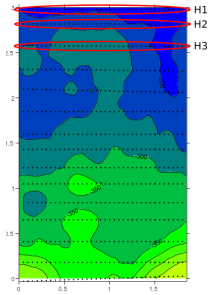

(a) HCP cartography on Pier G Face C – Automn

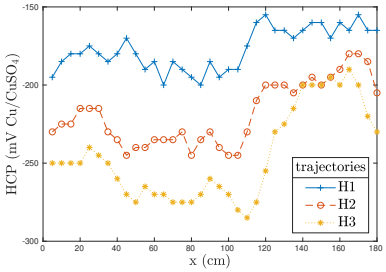

(b) Evidence of mean jumps in x=110 – 120 cm

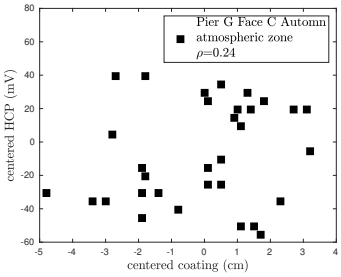

(c) Dependence of HCP on coating

Figure 14: Experimental validation in the case of a mean step - data illustration

is not likely to impact HCP on tidal and splash zones, frequently exposed to salt water, it is credible to identify it on atmospheric zone. Thus, we consider the H1 H2 and H3 trajectories non-stationary.

In the following, we test the applicability of SCAP-1D on H1 and compare correlation length estimations made on the three trajectories.

Application of SCAP-1D

First of all, we illustrate the necessity to take noise into account in the trajectory model. We apply the SCAP-1D procedure to both the raw and the 3-points-averaged H1 trajectory, which is supposed to derive from a piecewise-stationary GRF. Looking at experimental correlograms drawn on Figure 13c, it is clear that the moving average modifies the spatial variability properties (reduces it here). Thus, in the following, we only consider results coming from raw trajectories analysis.

Results from H1 analysis are given in Table 10 and illustrated in Figure 15a. We point out that the Matérn autocovariance model parameter ν is set to 8 (numerically equivalent to infinity and thus to gaussian model, see Table 2) in order to better fit the experimental covariogram. The centered signal seems ergodic, the mean is well-assessed and both the stationarity and the gaussiannity hypotheses cannot be rejected. This means H1 can indeed be considered as a stepped-gaussian trajectory. We however note high CoV for $\hat{l}_c$ and $\hat{\sigma}^2$, which are due to the limited number of measurement points (36) and especially to the low Signal Noise Ratio (SNR) of 0.52.

To confirm this, we compare previous assessments with estimations made from trajectories H2 and H3. Indeed, as all three studied trajectories have been measured in the same 40-cm high zone during the same day, it is reasonable to suppose they share same correlation length. Results are given in Table 10 and illustrated on Figure 15b and 15c.

Each studied trajectory is found to be ergodic, stationary and gaussian. Moreover, correlation lengths assessments are indeed quite similar, from 10.3 to 13.3 cm, with lower CoV of respectively 26 and 18 %. These are due to higher SNR of 5.24 and 21.72.

Thus, provided a sufficiently high SNR (above 5 according to this first experimental study) the SCAP-1D procedure is fully applicable to limited stepped experimental data with satisfying precisions on spatial variability assessment.

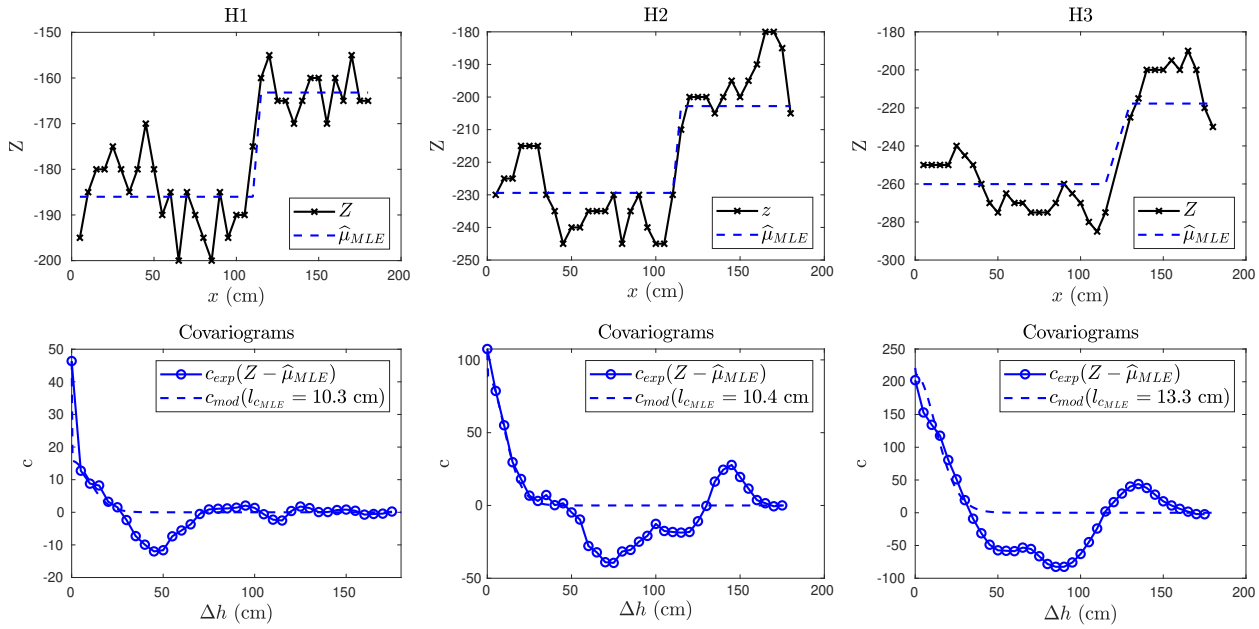

(a) H1 (b) H2 (c) H3

Figure 15: Experimental validation in the case of a mean step - results illustration

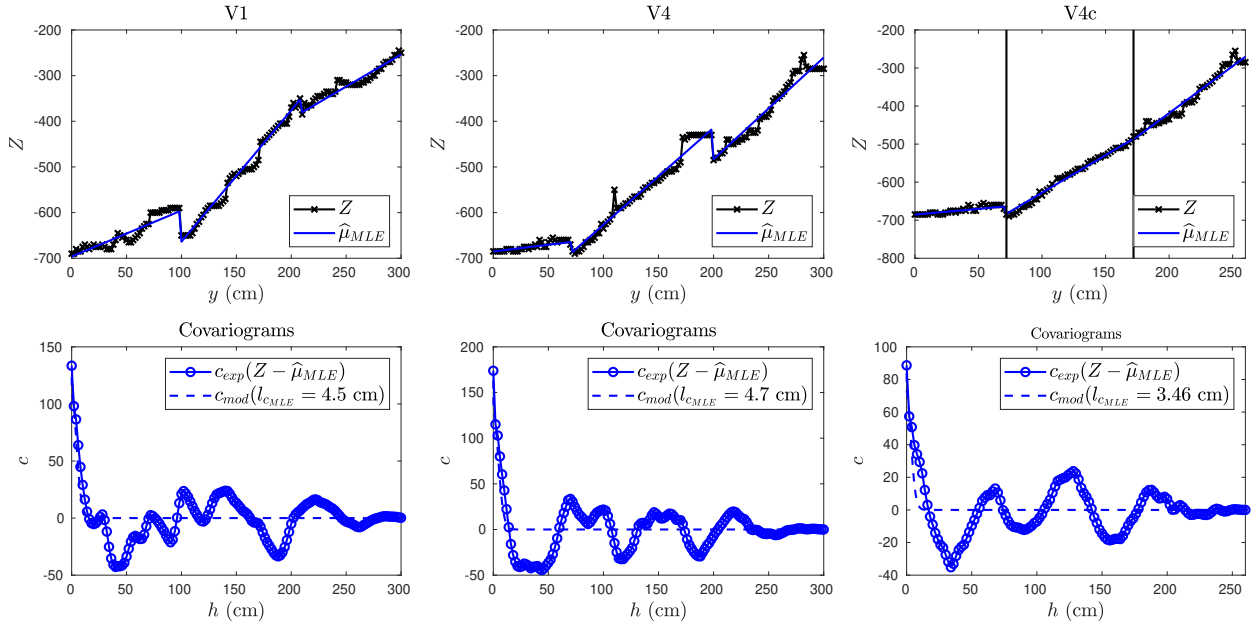

(a) V1 (b) V4 (c) V4 “cleaned”

Figure 16: Experimental validation in the case of a piecewise-linear step - results illustration

Table 10: Experimental valdation - results

SCAP-1D Results						
t	H1	H2	H3	V1	V4	V4c
Distribution law	GN	GN	GN	GN	GN	GN
Nb points	36	36	34	151	151	130
Nb changepoints	1	1	1	2	2	2
Regression degree	0	0	0	1	1	1
ν	8	8	8	8	8	8
Type 1 error	0.05	0.05	0.05	0.05	0.05	0.05
$\hat{\tau}^2$	30.51	16.95	9.73	13.97	34.55	11.35
$\hat{\sigma}$	4	9.4	14.4	10.46	11.34	8.51
$\hat{\sigma}^2$	15.77	88.74	211.37	109.38	128.61	72.36
$CR_{min}(\hat{\sigma}^2)$	0	23.83	49.92	68.67	77.63	46.34
$CR_{max}(\hat{\sigma}^2)$	35.93	153.65	372.83	150.09	179.59	98.38
$\hat{l}_c$	10.3	10.4	13.3	4.52	4.71	3.46
$CR_{min}(\hat{l}_c)$	1.00E-15	5.96	9.32	3.71	3.63	2.74
$CR_{max}(\hat{l}_c)$	23.34	14.79	17.17	5.33	5.8	4.18
h(χ^2-test)	FALSE	FALSE	FALSE	FALSE	TRUE	TRUE
h(KS-test)	FALSE	FALSE	FALSE	FALSE	TRUE	0
k	2.17	2.68	2.79	6.82	15.23	6.03
s	0.1	-0.42	0.27	1.37	2.37	0.64
h(KPSS-test)	FALSE	FALSE	FALSE	FALSE	FALSE	FALSE
h(ADF-test)	TRUE	TRUE	TRUE	TRUE	TRUE	TRUE
Results Analysis						
SNR	0.52	5.24	21.72	7.83	3.72	6.38
CoV $\hat{\sigma}^2$	0.78	0.44	0.46	0.23	0.24	0.22
CoV $\hat{l}_c$	0.77	0.26	0.18	0.11	0.14	0.13
t_{calc}(s)	0.47	1.78	0.87	3.53	3.36	2.16

5.4 CASE OF A PIECEWISE-LINEAR MEAN

Secondly, we validate the procedure in the experimental case of a piecewise-linear step for two similar trajectories.

Just as in the first experimental study, we limit environmental bias by selecting two trajectories of the same pier face and measured the same day. However, we focus here on vertical trajectories as their mean follow a piecewise-linear drift (Figure 17), with a slope depending on the corrosion zone (tidal, splash and atmospheric, see Table 9).

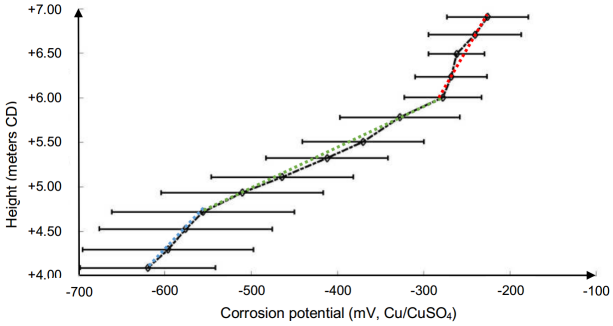

Figure 17: Piecewise-linear vertical trend of HCP [36]

Choice of tests trajectories

Among the available trajectories, we select those with drift which seems to correspond the most to the mean one. This allows to use the corrosion zones definition established by [36] .

The considerations above lead to test the applicability of SCAP-1D on two HCP trajectories measured in Spring on Pier G Face G, noted V1 and V4 (respectively measured at abscissa 0.2 m and 0.7 m). These are represented on Figure 18.

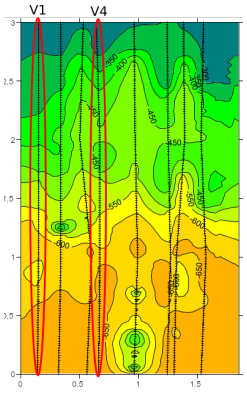

Figure 18: HCP cartography on Pier G Face G – Spring

Application of SCAP-1D

Results from V1 analysis are given in Table 10 and illustrated in Figure 16a. We keep $\nu = 8$ as we study the same quantity of interest. The centered signal seems ergodic, the mean is well assessed and both the stationarity and the gaussiannity hypotheses cannot be rejected. Moreover, the mean steps locations (y=1 m and x=2.10 m) correspond to the zones boundaries defined in Table 9. This means V1 can indeed be considered as a piecewise-linear gaussian trajectory. The correlation length and the standard deviation are precisely assessed with low CoV (11% and 23%). This is due to sizable number of points and SNR (151 and 7.83). To confirm this, we compare previous assessments with estimations made from trajectory V4, illustraded in Figures 16b and 16c.

In the first instance, V4 is found to be ergodic but non-stationary, as both χ^2-test and KS-test null hypotheses are rejected. However, by looking at the trajectory, we note an aberrant data at y=110 cm and two constant level of respectively -430 mV from y=172 cm to y=198 cm, and -285 mV from y=286 cm to y=300 cm. However, even if SCAP-1D can handle such mean shapes by simple modification of the nodal matrix A (Example 1), taking these additional steps into account in the trajectory model would add two parameters and considerably affect the estimators accuracy. Thus, we create a "cleaned" study trajectory (noted V4c) by removing both the aberrant data and these intermediate levels from V4. The new trajectory gets 130 points and the information of steps locations is saved to perform the following assessments.

V4c is then found to be ergodic, stationary and gaussian, even if the χ^2-test is not valid (see Table 10). Moreover, correlation length and standard deviation assessments are indeed quite similar to V1 estimations (respectively 4.71 cm and 11.34 mV against 4.52 cm and 10.46 mV) with still low CoV (14% and 24%), even if the SNR is lower (3.72).

Thus, providing suitably conditioned data (without aberrant values and precise correspondence between model and measurements evolution), the SCAP-1D procedure is fully applicable to piecewise-linear experimental data with satisfying precision on spatial variability assessment.

6 CONCLUSIONS

This paper proposes a rigorous spatial variability assessment procedure adapted to unidimensional piecewise-trend-stationary trajectories, called SCAP-1D. This strategy may enable structures stakeholders to assess an additional information from sensors after diagnosis campaigns as it allows to precisely determine the correlation length of quantities of interest, such as chloride concentration, resistivity or corrosion potential. It may also be of great interest for the design of Structure Health Monitoring systems.

While spatial variability is often estimated through approximate methods, our algorithm checks each mathematical hypothesis required to perform its assessment while removing non-stationarities due to piecewise-linear environmental

effects, preventing calculation errors up to 100%.

Here, after an exhaustive presentation of the theoretical aspects of SCAP-1D (covering piecewise-assessment techniques, normality tests and stationarity tests), numerical studies have been carried out to validate its ability to accurately estimate spatial variability of a gaussian random field in three typical cases of a constant mean, a stepped-mean and a bilinear mean.

It has been shown that, (i) provided the stationary trajectory is ergodic, SCAP-1D precisely estimates the mean, the variance and the correlation length, (ii) the ratio step amplitude/standard deviation pilots the efficiency of SCAP-1D with a minimum detection value around 2, (iii) the slope steps should be above 30 times the ratio standard deviation/domain size. It has also been highlighted that initializing the correlation length through Least Square Estimation significantly reduces the procedure execution time, and that the trajectory size should be significantly higher than the expected correlation length in order to validate the ergodicity hypothesis.

The procedure has finally been tested on Half-Cell Corrosion Potential measurements carried out on the Île de Ré bridge. Measurement noise has been taking into account with simple Maximum Likelihood estimators adjustments. This led to the following conclusions : (i) SCAP-1D is fully capable of determining mean and slope steps on limited experimental data (ii) Using SCAP-1D on a unique trajectory with few points (about 30 points) is enough to accurately determine material spatial variability, on the conditions of limited noise (SNR above 5), filtered aberrant data, accurate mean model and homogeneous properties along the structure.

For future works, it is of a great interest to extend the procedure to non-uniform and two-dimensional grids which may lead to detect non-stationarities on whole surfaces without constraining the measurements locations. We also point out that the SCAP-1D procedure currently gets numerous parameters which may highly impact its results if not fully understood. Its partial automation with adequate analysis tools is thus of interest to get it used by engineers and structures stakeholders.

To achieve this goal, a systematic statistical evaluation of the performance of the algorithm should also be carried out in order to precisely characterize the influence of the random field model, the auto-covariance function and the SCAP-1D parameters on the accuracy and the efficiency of the algorithm. This could guide future users in the choice of global settings of the procedure.

ACKNOWLEDGMENTS

The “DéCoF-Ré” project meaning Decision Corrosion Reliability on the Ile de Ré Bridge was coordinated by V. Bouteiller from IFSTTAR in the period 2014-2018. The investigations and results reported herein were supported by the Charente Maritime Department, SIXENSE-Concrete company, the French Institute of Science and Technology for Transport, Development and Networks (IFSTTAR), the Centre For Studies and Expertise on Risks, Environment, Mobility, and Urban and Country planning (CEREMA), Nantes University (GeM Laboratory) and CAPACITES SAS.

The authors would like to thank the team of the DéCoF-Ré Project: V. Bouteiller, L. Gaillet, B. Godart, W. Traverst, P. Boujard, N. Coulaty-Chin, A. Orcesi, Y. El Rabbih, X. Derobert, M. Sissoko (IFSTTAR); B. Thauvin, R. Queguiner, S. Pasquiet, P. Boulaire, M. Rebours, C. Naudat (CEREMA DterOuest); J. Schneider, F. Landrin and V. Queyrat (Cerema Dter Ile de France), J-F. Barthélémy (CEREMA Dtec ITM); M. Roche (Nantes University); L. Bourreau, M. Brouxel, S. Naar (SIXENSE-Concrete), A. Audouin-Dubreuil, F. Lavoute, M. Barbier (Département de la Charente Maritime); F. Gazet (Dekra). They also thank the team of the vessel for their help.

References

[1] J. van Noortwijk, A survey of the application of gamma processes in maintenance, Reliability Engineering & System Safety 94 (1) (2009) 2–21. doi:10.1016/j.ress.2007.03.019.
URL http://linkinghub.elsevier.com/retrieve/pii/S0951832007001111

[2] C. Gomez-Cardenas, Z. Sbartaï, J. Balayssac, V. Garnier, D. Breysse, New optimization algorithm for optimal spatial sampling during non-destructive testing of concrete structures, Engineering Structures 88 (2015) 92–99. doi:10.1016/j.engstruct.2015.01.014.
URL http://linkinghub.elsevier.com/retrieve/pii/S0141029615000218

[3] F. Schoefs, E. Bastidas-Arteaga, T. Tran, G. Villain, X. Derobert, Characterization of random fields from NDT measurements: A two stages procedure, Engineering Structures 111 (2016) 312–322. doi:10.1016/j.engstruct.2015.11.041.
URL http://linkinghub.elsevier.com/retrieve/pii/S0141029615007476

[4] M. Oumouni, F. Schoefs, An adaptative approach for spatial variability assessment of structures from distributed measurements, Under Submission.

[5] N. A. C. Cressie, Geostatistics, in: Statistics for Spatial Data, Wiley-Blackwell, 2015, pp. 27–104. doi:10.1002/9781119115151.ch2.
URL https://onlinelibrary.wiley.com/doi/abs/10.1002/9781119115151.ch2

[6] A. J. O'Connor, O. Kenshel, Experimental Evaluation of the Scale of Fluctuation for Spatial Variability Modeling of Chloride-Induced Reinforced Concrete Corrosion, Journal of Bridge Engineering 18 (1) (2013) 3–14. doi:10.1061/(ASCE)BE.1943-5592.0000370.
URL http://ascelibrary.org/doi/10.1061/%28ASCE%29BE.1943-5592.0000370

[7] N. R. Ravahatra, F. Duprat, F. Schoefs, T. de Larrard, E. Bastidas-Arteaga, Assessing the Capability of Analytical Carbonation Models to Propagate Uncertainties and Spatial Variability of Reinforced Concrete Structures, Frontiers in Built Environment 3. doi:10.3389/fbuil.2017.00001.
URL http://journal.frontiersin.org/article/10.3389/fbuil.2017.00001/full

[8] M. G. Stewart, A. Al-Harthy, Pitting corrosion and structural reliability of corroding RC structures: Experimental data and probabilistic analysis, Reliability Engineering & System Safety 93 (3) (2008) 373–382. doi:10.1016/j.ress.2006.12.013.
URL http://www.sciencedirect.com/science/article/pii/S0951832007000099

[9] L. Bourreau, V. Bouteiller, F. Schoefs, L. Gaillet, B. Thauvin, J. Schneider, S. Naar, Uncertainty assessment of concrete electrical resistivity measurements on a coastal bridge, Structure and Infrastructure Engineering (2019) 1–11doi:10.1080/15732479.2018.1557703.
URL https://www.tandfonline.com/doi/full/10.1080/15732479.2018.1557703

[10] T. Desbois, S. Pasquiet, R. Queguiner, B. Thauvin, Poste charbonnnier Grand Port Maritime de Nantes Saint-Nazaire Montoir de Bretagne : Synthèse des mesures réalisées sur site avant réparation de l'ouvrage par protection cathodique, Tech. rep., CETE de l'Ouest (Dec. 2012).

[11] Y. Dwivedi, S. Subba Rao, A test for second-order stationarity of a time series based on the discrete Fourier transform: TEST FOR SECOND-ORDER STATIONARITY, Journal of Time Series Analysis 32 (1) (2011) 68–91. doi:10.1111/j.1467-9892.2010.00685.x.
URL http://doi.wiley.com/10.1111/j.1467-9892.2010.00685.x

[12] R. Ranta, V. Louis-Dorr, C. Heinrich, D. Wolf, F. Guillemin, Débruitage par ondelettes et segmentation de signaux non-stationnaires: réinterprétation d'un algorithme itératif et application à la phonoentérographie, Traitement du signal 20 (2) (2003) 119–135.

[13] S. Mallat, W. Hwang, Singularity detection and processing with wavelets, IEEE Transactions on Information Theory 38 (2) (1992) 617–643. doi:10.1109/18.119727.
URL http://ieeexplore.ieee.org/document/119727/

[14] E. S. Page, CONTINUOUS INSPECTION SCHEMES, Biometrika 41 (1-2) (1954) 100–115. doi:10.1093/biomet/41.1-2.100.
URL https://academic.oup.com/biomet/article/41/1-2/100/456627

[15] D. V. Hinkley, Inference about the change-point from cumulative sum tests, Biometrika 58 (3) (1971) 509–523. doi:10.1093/biomet/58.3.509.
URL https://academic.oup.com/biomet/article/58/3/509/233432

[16] M. Basseville, Detecting changes in signals and systems – a survey, Automatica 24 (3) (1988) 309–326. doi:10.1016/0005-1098(88)90073-8.

[17] J. Labeyrie, Stationary and transient states of random seas, Marine Structures 3 (1) (1990) 43–58. doi:10.1016/0951-8339(90)90020-R.
URL http://linkinghub.elsevier.com/retrieve/pii/095183399090020R

[18] R. Killick, P. Fearnhead, I. A. Eckley, Optimal Detection of Changepoints With a Linear Computational Cost, Journal of the American Statistical Association 107 (500) (2012) 1590–1598. doi:10.1080/01621459.2012.737745.
URL https://amstat.tandfonline.com/doi/abs/10.1080/01621459.2012.737745

[19] B. Jackson, J. Scargle, D. Barnes, S. Arabhi, A. Alt, P. Gioumousis, E. Gwin, P. San, L. Tan, Tun Tao Tsai, An algorithm for optimal partitioning of data on an interval, IEEE Signal Processing Letters 12 (2) (2005) 105–108. doi:10.1109/LSP.2001.838216.
URL http://ieeexplore.ieee.org/document/1381461/

[20] D. Kwiatkowski, P. C. B. Phillips, P. Schmidt, Y. Shin, Testing the null hypothesis of stationarity against the alternative of a unit root: How sure are we that economic time series have a unit root?, Journal of Econometrics 54 (1) (1992) 159–178. doi:10.1016/0304-4076(92)90104-Y.
URL http://www.sciencedirect.com/science/article/pii/030440769290104Y

[21] D. A. Dickey, W. A. Fuller, Likelihood Ratio Statistics for Autoregressive Time Series with

a Unit Root, Econometrica 49 (4) (1981) 1057. doi:10.2307/1912517.
URL http://www.jstor.org/stable/1912517?origin=crossref

[22] T. J. Sweeting, Uniform Asymptotic Normality of the Maximum Likelihood Estimator, The Annals of Statistics 8 (6) (1980) 1375–1381.
URL http://www.jstor.org/stable/2240949

[23] K. V. Mardia, R. J. Marshall, Maximum Likelihood Estimation of Models for Residual Covariance in Spatial Regression, Biometrika 71 (1) (1984) 135–146. doi:10.2307/2336405.
URL http://www.jstor.org/stable/2336405

[24] M. H. Faber, Statistics and Probability Theory, Vol. 18 of Topics in Safety, Risk, Reliability and Quality, Springer Netherlands, Dordrecht, 2012. doi:10.1007/978-94-007-4056-3.
URL http://link.springer.com/10.1007/978-94-007-4056-3

[25] U. K. Müller, Size and power of tests of stationarity in highly autocorrelated time series, Journal of Econometrics 128 (2) (2005) 195–213. doi:10.1016/j.jeconom.2004.08.012.
URL http://linkinghub.elsevier.com/retrieve/pii/S030440760400154X

[26] D. N. DeJong, J. C. Nankervis, N. E. Savin, C. H. Whiteman, The power problems of unit root test in time series with autoregressive errors, Journal of Econometrics 53 (1-3) (1992) 323–343. doi:10.1016/0304-4076(92)90090-E.

[27] D. Rios Insua, F. Ruggeri, M. P. Wiper, Bayesian Analysis of Stochastic Process Models, 1st Edition, Wiley Series in Probability and Statistics, Wiley, 2012. doi:10.1002/9780470975916.
URL https://onlinelibrary.wiley.com/doi/book/10.1002/9780470975916

[28] J.-F. Coeurjolly, E. Porcu, Fast and exact simulation of complex-valued stationary Gaussian processes through embedding circulant matrix, Journal of Computational and Graphical Statistics (2017) 0–0doi:10.1080/10618600.2017.1385468.
URL https://amstat.tandfonline.com/doi/abs/10.1080/10618600.2017.1385468

[29] F. Schoefs, A. Clément, A. Nouy, Assessment of ROC curves for inspection of random fields, Structural Safety 31 (5) (2009) 409–419. doi:10.1016/j.strusafe.2009.01.004.
URL http://www.sciencedirect.com/science/article/pii/S0167473009000034

[30] I. Othmen, S. Bonnet, F. Schoefs, Statistical investigation of different analysis methods for chloride profiles within a real structure in a marine environment, Ocean Engineering 157 (2018) 96–107. doi:10.1016/j.oceaneng.2018.03.040.
URL http://linkinghub.elsevier.com/retrieve/pii/S0029801818303056

[31] F. Schoefs, M. Oumouni, R. Clerc, I. Othmen, S. Bonnet, Statistical analysis and probabilistic modeling of chloride ingress spatial variability in concrete coastal infrastructures, in: Edition 4, Split, Croatie, Editions Paralia, Split, Croatia, 2017, pp. 229–234. doi:10.5150/cmcm.2017.042.
URL http://www.paralia.fr/cmcm/e04-42.pdf

[32] J. I. Myung, M. A. Pitt, Model Comparison Methods, in: Methods in Enzymology, Vol. 383, Elsevier, 2004, pp. 351–366. doi:10.1016/S0076-6879(04)83014-3.
URL https://linkinghub.elsevier.com/retrieve/pii/S0076687904830143

[33] N. T. Nguyen, Z.-M. Sbartaï, J.-F. Lataste, D. Breysse, F. Bos, Assessing the spatial variability of concrete structures using NDT techniques – Laboratory tests and case study, Construction and Building Materials 49 (Supplement C) (2013) 240–250. doi:10.1016/j.conbuildmat.2013.08.011.
URL http://www.sciencedirect.com/science/article/pii/S0950061813007411

[34] Y. Sahraoui, A. Chateauneuf, The effects of spatial variability of the aggressiveness of soil on system reliability of corroding underground pipelines, International Journal of Pressure Vessels and Piping 146 (2016) 188–197. doi:10.1016/j.ijpvp.2016.09.004.
URL https://linkinghub.elsevier.com/retrieve/pii/S0308016116303088

[35] L. Bourreau, Diagnostic de corrosion sur ouvrage : fiabilité et aide à la décision, thesis, Université de Nantes (Dec. 2017).
URL http://www.theses.fr/2017NANT4083

[36] L. Bourreau, L. Gaillet, V. Bouteiller, F. Schoefs, B. Thauvin, J. Schneider, S. Naar, Assessment of exposure-corrosion zones for reinforced concrete structures in marine environment 16.

A Appendix A : Iterative Algorithm of Maximum Likelihood Estimation of the mean and geostatistic properties - case of a Gaussian Random Field

Data:
$\boldsymbol{Z}$: trajectory
Input:
$\boldsymbol{A}$: nodal piecewise-linear function matrix
$f_{cov}(\boldsymbol{x}, l_c)$: supposed auto-covariance function of $\boldsymbol{G}$
l_{c0} : initial value of the correlation length
$\hat{\boldsymbol{\mu}}_0$: initial vector of the piecewise-linear mean
$\hat{\sigma}_0^2$: initial value of the variance
ε : initial error on geostatistical parameter evaluation
tol : tolerance on geostatistical parameter evaluation
Result:
$\hat{\boldsymbol{G}}$: random gaussian part of $\boldsymbol{Z}$ assessment
$\hat{\boldsymbol{\mu}}$: assessment of the piecewise-polynomial mean of $\boldsymbol{Z}$
$\hat{\sigma}^2$: assessment of the constant variance of $\boldsymbol{G}$
$\hat{\boldsymbol{C}}$: assessment of the auto-covariance matrix of $\boldsymbol{Z}$
$\hat{l}_c$: assessment of the constant correlation length of $\boldsymbol{G}$
$\hat{\boldsymbol{\alpha}}$: assessment of the regression coefficients of μ
$\boldsymbol{R}$: modeled autocorrelation matrix of $\boldsymbol{G}$
while $\varepsilon <$ tol **do**

model $\boldsymbol{G}$ autocorrelation matrix ;

$$\boldsymbol{R} = \boldsymbol{R}(f_{cov}, \boldsymbol{x}, l_{c0})$$

assess the piecewise-polynomial mean via MLE ;

$$\hat{\boldsymbol{\alpha}} = \frac{\boldsymbol{Z}'\hat{\boldsymbol{R}}^{-1}\boldsymbol{A}}{\boldsymbol{A}'\hat{\boldsymbol{R}}^{-1}\boldsymbol{A}} \quad ; \quad \hat{\boldsymbol{\mu}} = \boldsymbol{A}\hat{\boldsymbol{\alpha}}$$

assess the variance of $\boldsymbol{G}$ via MLE ;

$$\hat{\sigma}^2 = \frac{1}{n}(\boldsymbol{Z} - \hat{\boldsymbol{\mu}})' \boldsymbol{R}^{-1} (\boldsymbol{Z} - \hat{\boldsymbol{\mu}})$$

assess the gaussian random part of the trajectory and the auto-covariance matrix ;

$$\hat{\boldsymbol{G}} = \frac{\boldsymbol{Z} - \hat{\boldsymbol{\mu}}}{\sqrt{\hat{\sigma}^2}} \quad ; \quad \hat{\boldsymbol{C}} = \hat{\sigma}^2.\boldsymbol{R}$$

assess the correlation length of $\hat{\boldsymbol{G}}$ via MLE, with L defined as the likelihood function of parameter l_c of multivariate normal distribution ;

$$\hat{l}_c = \underset{l_c}{\operatorname{argmax}} L(l_c) = \underset{l_c}{\operatorname{argmin}} \left[-2\log\left(L(l_c)\right)\right] = \underset{l_c}{\operatorname{argmin}} \left[\log\left(|\hat{\boldsymbol{C}}|\right) + \hat{\boldsymbol{G}}'\hat{\boldsymbol{C}}^{-1}\hat{\boldsymbol{G}}\right]$$

update the error on geostatistical parameter evaluation

$$\varepsilon = \|\hat{\sigma}^2 - \hat{\sigma}_0^2\| \Leftrightarrow \varepsilon = \|\hat{l}_c - \hat{l}_{c0}\| \Leftrightarrow \varepsilon = \|\hat{\boldsymbol{\mu}} - \hat{\boldsymbol{\mu}}_{\boldsymbol{0}}\|$$

update initial geostatistical parameters

$$\hat{\boldsymbol{\mu}}_0 = \hat{\boldsymbol{\mu}} \quad ; \quad \hat{\sigma}_0^2 = \hat{\sigma}^2 \quad ; \quad l_{c0} = l_c$$

end

B Appendix B : Iterative Algorithm of Maximum Likelihood Estimation of the mean and geostatistic properties - case of a Gaussian Random Field with additive noise

Data:
$\boldsymbol{Z}$: trajectory
Input:
$\boldsymbol{A}$: nodal piecewise-linear function matrix
$f_{cov}(\boldsymbol{x}, l_c)$: supposed auto-covariance function of $\boldsymbol{G}$
$\hat{l}_{c0}$: initial value of the correlation length
$\hat{\boldsymbol{\mu}}_0$: initial vector of the piecewise-linear mean
$\hat{\sigma}_0^2$: initial value of the variance
$\hat{\tau}_0^2$: initial value of the noise
ε : initial error on geostatistical parameter evaluation
tol : tolerance on geostatistical parameter evaluation
Result:
$\hat{\boldsymbol{\mu}}$: assessment of the piecewise-polynomial mean of $\boldsymbol{Z}$
$\hat{\sigma}^2$: assessment of the constant variance of $\boldsymbol{Z} - \boldsymbol{\mu}$
$\hat{\tau}^2$: assessment of the constant noise in $\boldsymbol{Z} - \boldsymbol{\mu}$
$\hat{\boldsymbol{C}}$: assessment of the auto-covariance matrix of $\boldsymbol{Z}$
$\hat{l}_c$: assessment of the constant correlation length of $\boldsymbol{Z} - \boldsymbol{\mu}$
$\hat{\boldsymbol{\alpha}}$: assessment of the regression coefficients of $\boldsymbol{\mu}$
while $\varepsilon <$ tol **do**

model $\boldsymbol{C}$ autocovariance matrix ;

$$\boldsymbol{C} = \hat{\sigma}_0^2 . \boldsymbol{R}\left(f_{cov}, \boldsymbol{x}, \hat{l}_{c0}\right) + \hat{\tau}_0^2 . \mathbf{1}_n$$

assess the piecewise-polynomial mean via MLE ;

$$\hat{\boldsymbol{\alpha}}' = \frac{\boldsymbol{Z}'\boldsymbol{C}^{-1}(\boldsymbol{A}\mathbf{1}_n)}{(\boldsymbol{A}\mathbf{1}_n)'\boldsymbol{C}^{-1}(\boldsymbol{A}\mathbf{1}_n)} \quad ; \quad \hat{\boldsymbol{\mu}} = \boldsymbol{A}\hat{\boldsymbol{\alpha}}$$

assess the variance, noise and correlation length via MLE ;

$$\left(\hat{\sigma}^2, \hat{\tau}^2, \hat{l}_c\right) = \underset{\sigma^2, \tau^2, l_c}{\operatorname{argmin}} \left[\log(|\boldsymbol{C}(\sigma^2, \tau^2, l_c)|) + \left((\boldsymbol{Z} - \boldsymbol{A}\boldsymbol{\alpha})'\boldsymbol{C}(\sigma^2, \tau^2, l_c)^{-1}(\boldsymbol{Z} - \boldsymbol{A}\boldsymbol{\alpha})\right)\right]$$

update the error on geostatistical parameter evaluation

$$\varepsilon = \|\hat{\sigma}^2 - \hat{\sigma}_0^2\| \Leftrightarrow \varepsilon = \|\hat{l}_c - \hat{l}_{c0}\| \Leftrightarrow \varepsilon = \|\hat{\boldsymbol{\mu}} - \hat{\boldsymbol{\mu}}_{\mathbf{0}}\|$$

update initial geostatistical parameters

$$\hat{\boldsymbol{\mu}}_0 = \hat{\boldsymbol{\mu}} \quad ; \quad \hat{\sigma}_0^2 = \hat{\sigma}^2 \quad ; \quad \hat{l}_{c0} = l_c$$

end